

REMARKS

Claims 1-3 and 5-13 are pending in this application. By this Amendment, the specification has been amended to attend to minor informalities. Applicants submit that no new matter is presented by these amendments.

Objections to the Specification

The specification was objected to because paragraph [00039] referred to claims. In response to this objection, Applicants have removed the reference to claims 1-6 from paragraph [00039].

The Office Action also pointed out that the trademarks Beacon® and GraphPad Prism® were used in the specification, and that they should be capitalized and accompanied by generic terminology. Although this was not specifically indicated to be an objection, Applicants have amended paragraphs [00030] and [00049] as indicated. Copies of publicly-available literature for the Beacon® 2000 and GraphPad Prism® products are attached.

Withdrawal of the outstanding objection to the specification is therefore respectfully requested.

Rejections under 35 U.S.C. § 112

Claims 6-13 were rejected under 35 U.S.C. § 112, first paragraph, as allegedly containing new matter. Specifically, the feature wherein the subunits are selected from the group consisting of the Arp2/3 complex and the Ena/VASP family of proteins, and the feature wherein the kit comprises subunits of the Arp2/3 complex and the Ena/VASP family of proteins, were not considered to be supported by the specification. The Office

Action takes the position that the specification only teaches the Arp2/3 complex and the Ena/VASP family of proteins in a general fashion, and does not specifically disclose the step of adding either of these compounds in order to activate endogenous actin polymerization or a kit comprising these subunits. Applicants respectfully traverse this rejection.

In response to this rejection, Applicants initially submit that this rejection does not appear to be a new matter rejection, as it was characterized in the Office Action. The Arp2/3 complex and Ena/VASP family of proteins, which are described as being involved in mechanisms for regulating actin polymerization, are clearly disclosed and are not new matter. See, for example, paragraphs [00006], [00007], and [00022] of the specification.

It appears that the rejection may actually be based on an alleged lack of written description, but the Office Action has not met the initial burden of establishing by a preponderance of evidence why a person skilled in the art would not recognize in Applicants' disclosure a description of the invention defined by the claims. See *In re Wertheim*, 541 F.2d 257, 263, 191 U.S.P.Q. 90, 97 (CCPA 1976). Regardless, Applicants submit that one skilled in the art would understand how to incorporate the Arp2/3 complex and Ena/VASP family of proteins into the presently-claimed methods to activate endogenous actin polymerization, which include a step of adding one or more substances to activate endogenous actin polymerization, based on the disclosure provided in the specification and the knowledge available at the time the presently-claimed invention was made.

Claims 8-11 were rejected under 35 U.S.C. § 112, second paragraph, as allegedly being indefinite for failing to particularly point out and distinctly claim the

subject matter which Applicants regard as their invention. Claims 8-11 relate to the application of the methods of claims 1-3 and 5-6 to the evaluation of the invasive character of the cells, evaluation of the oncogenicity of the cells, and prediction of the sensitivity of the cells to an anticancer treatment. The Office Action takes the position that these are goals, rather than methods, and that it is unclear how they will be accomplished. Applicants respectfully traverse this rejection.

In response to this rejection, Applicants submit that one skilled in the art would understand that by carrying out the methods for analyzing the tumor aggressivity of cancerous cells set forth in claims 1-3 and 5-6, the invasive character of the cells, oncogenicity of the cells, and sensitivity of the cells to an anticancer treatment would necessarily also be determined, as these are components of tumor aggressivity. See, for example, paragraphs [00016] and [00032] of the specification. One skilled in the art would understand that no additional steps are required in order to carry out these methods.

Withdrawal of these rejections is therefore respectfully requested.

Rejection under 35 U.S.C. § 103(a)

Claims 1-3 and 5-8 were rejected under 35 U.S.C. § 103(a) as allegedly being unpatentable over Tellam et al. (1986) in view of Menu et al. (2002). Applicants respectfully traverse this rejection.

The Presently-Claimed Invention

The presently-claimed invention relates to methods of analyzing the tumor aggressivity of cancerous cells consisting of the measurement of the quantity of

polymerized actin in the steady state in a lysate of the said cells, wherein the measurement of the quantity of actin in the steady state is carried out by static fluorescence polarization in the presence of actin monomers bound to a fluorochrome, the monomers being incorporated into the actin filaments (actin F) formed during the endogenous actin polymerization of the lysate. The presently-claimed invention also relates to methods of identifying molecules likely to have anti-cancer activity, methods of evaluating cancer cells to determine their invasiveness, oncogenicity, and sensitivity to cancer treatments, as well as kits for carrying out these methods.

The dynamic properties of the cytoskeleton render the analysis of the polymerization of the actin extremely complex. It is a significant challenge to find a model of actin polymerization that is representative of the condition of a living cell.

Applicants attained this objective by means of a method which consists of measuring the quantity of polymerized actin in the steady state, which takes into account the results of all the mechanisms for regulating polymerization and depolymerization of actin filaments.

More precisely, the method of the present invention closely approximates the physiological conditions in the cell:

- (i) Applicants add the polymerization buffer at conditions that are near the physiological conditions in cell, which is required for polymerization;
- (ii) Alexa 488-actin monomers are used as tracers that are incorporated in the actin filaments during actin polymerization, and then in a very small quantity (in nanomolar concentration);
- (iii) Applicants use a cellular lysate in which the proteins remain associated with actin.

Furthermore, the methods of the present invention permit the measurement of the dynamism of actin, in particular by the measurement of K_{obs} (the apparent constant), not only a measurement at a given time. The potential of actin polymerization is lower in tumor cells as compared to normal cell lysates. Therefore, measurement of the dynamism of actin permits observation of the effect of anti-tumor drugs on the restoration of actin polymerization in tumoral cell lysate.

Rejection Based on Tellam et al. and Menu et al.

The Office Action takes the position that Tellam et al. discloses a method for determining the nucleating activity in tumorigenic cells, wherein tumorigenic cells are lysed in non-denaturing conditions and centrifuged to remove cellular debris. Fluorochrome-labeled actin monomers are added to the lysate along with substances necessary for the polymerization of endogenous actin and protection of the lysate proteins. The quantity of polymerized actin monomers incorporated into the actin filaments from the cell lysate of tumorigenic cells is measured, and is compared to the reference quantity of polymerized actin from non-tumorigenic cells. Tellam et al. is also cited for disclosing a cell re-suspension medium, substances necessary for the endogenous actin polymerization and protection of the lysate proteins, solutions of actin monomers labeled with a fluorochrome, and extracts of tumorigenic and non-tumorigenic cells and reaction buffers. The Office Action further indicated that while Tellam et al. is directed to the measurement of exogenous skeletal muscle actin, it discloses that the higher actin nucleating activity seen in tumorigenic cells results from the lower level of total endogenous cellular actin within the tumorigenic cells.

However, the Office Action admits that Tellam et al. fails to disclose or suggest a method wherein the quantity of polymerized actin corresponds to the sum of all of the F-form actin, wherein the measurement of the quantity of actin in the steady state is carried out by static fluorescence polarization in the presence of actin monomers bound to a fluorochrome which are added to the cellular lysate in a proportion ranging from 1/80th and 1/1600th in relation to the quantity of endogenous actin, the monomers being incorporated into actin filaments (F-actin) formed during endogenous actin polymerization of the lysate, wherein the method is used to evaluate the invasive character of the cells, or a kit including a cell re-suspension medium for the cell lyses, substances necessary for the endogenous actin polymerization and the protection of the lysate proteins, a solution of actin monomers bound to a fluorochrome, an actin polymerization solution, a general actin solution, and optionally the extracts of aggressive and nonaggressive reference cells.

Menu et al. is cited for allegedly disclosing a method of determining the tumor aggressivity of cancerous cells by measuring the quantity of polymerized F-actin in the steady state of the lysate of the cells, comparing the value of the quantity of polymerized F-actin in the cancerous cells to a reference value of non-migrating cells, exposing the cells to the actin polymerization inhibitor latrunculin-A, and determining the capacity of the latrunculin-A to restore the quantity of polymerized actin in the steady state to that of the non-migrating cells. Menu et al. is also cited for allegedly disclosing that F-actin becomes polarized when the cells are migrating, in contrast to non-migrating cells, and that this polarization can be visualized by fluorescence and confocal laser scanning microscopy and quantified by fluorometry and flow cytometry.

Applicants submit that Tellam et al. discloses the use of a large quantity of purified pyrene actin (5 μ M) in their test. Therefore, the test is ***not conducted under physiological conditions***. This abnormally accelerates the initial rate of skeletal muscle purified actin polymerization. See p.1285, last paragraph. Furthermore, this method only permits measurement of ***part*** of the actin polymerization (i.e., the first step, nucleation).

On the contrary, the method of the presently-claimed invention allows:

- (i) ***near physiological conditions***, because we use actin issued from the cell (and not the purified pyrene actin added in the Tellam et al. method); and
- (ii) measurement of the ***global kinetics*** of actin polymerization.

The Office Action states that Menu et al. disclose "direct measurement of polymerized endogenous F-actin, no extraneous actin being added in the method". The Applicant respectfully disagrees because Menu et al. measures ***only*** the actin F (filament) content in the cell ***at a given time***.

In contrast, the method of the presently-claimed invention is able to measure the actin dynamic in the cell because:

- (i) a cellular lysate in which the proteins remain associated with actin is used; and
- (ii) the constant K_{obs} , which is a measure of the evolution of actin polymerization ***in real time***, is measured.

Menu et al. discloses a completely different method which ***does not*** represent the reality of the actin dynamics in the cell.

Accordingly, the combination of Tellam et al. and Menu et al. fail to measure the quantity of actin present in the steady state, as set forth in the presently-claimed invention.

To demonstrate this difference, Applicants refer to the fact that the actin content in 3T3 cells and 3T3EF cells was found to be the same (see article by Amsellem et al., at page 4, column 1, a copy of which is enclosed), whereas Applicants have observed during testing that the kinetics of actin polymerization of these cell lysates are completely different, i.e., the ΔmA and K_{obs} values are different (see Table 2 of the specification). This is due to the fact that the lysate Applicants use in their tests is at close to physiological conditions, and therefore it is possible to observe the impact of actin associated protein on the kinetics of actin polymerization.

So even if one of ordinary skill in the art would understand from the disclosure of Tellam et al. that there is a difference in actin polymerization between tumorigenic cells and non-tumorigenic cells, by combining Menu et al. (or any publications or documents of the art) he would not have known how to measure the polymerized actin at *near physiological conditions* or how to measure the *dynamics of the polymerized actin in real time*. These criteria must be met in order to carry out the presently-claimed methods for screening on the basis of the actin polymerization.

In view of the remarks set forth above, Applicants respectfully submit that Tellam et al. and Menu et al., fail to disclose or suggest the features of the pending claims. As such, Applicants respectfully request that the rejection of claims 1-3 and 5-8 as allegedly being unpatentable over the combination of Tellam et al. and Menu et al. be withdrawn.

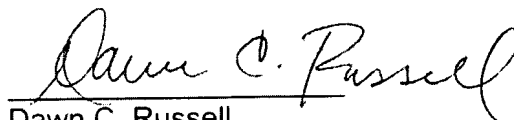
CONCLUSION

In view of the foregoing, reconsideration of the application, withdrawal of the outstanding rejections, allowance of Claims 1-3 and 5-13, and the prompt issuance of a Notice of Allowability are respectfully solicited.

Should the Examiner believe anything further is desirable in order to place this application in better condition for allowance, the Examiner is requested to contact the undersigned at the telephone number listed below.

In the event this paper is not considered to be timely filed, Applicants respectfully petition for an appropriate extension of time. Any fees for such an extension, together with any additional fees that may be due with respect to this paper, may be charged to counsel's Deposit Account No. 01-2300, **referencing Attorney Dkt. No. 021305-00214.**

Respectfully submitted,



Dawn C. Russell
Attorney for Applicants
Registration No. 44,751

Enclosures:

Beacon® 2000 brochure
Excerpt from GraphPad Prism® online product description
Amsellem et al. article

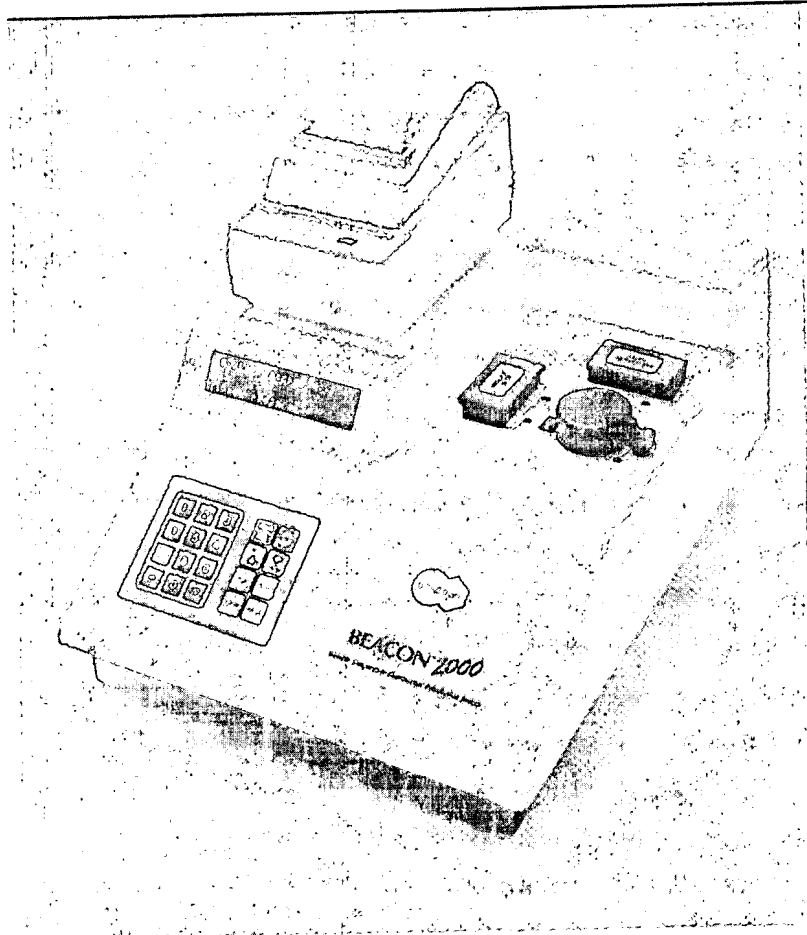
Customer No. 004372

ARENT FOX LLP
1050 Connecticut Avenue, N.W.,
Suite 400
Washington, D.C. 20036-5339
Tel: (202) 857-6000
Fax: (202) 638-4810

DCR/vdb



Ultra-sensitive,
ultra-convenient, ultra-simple



The Beacon™ 2000
Fluorescence Polarization
Instrument provides:

- Rapid and precise measurements
- Ultrasensitive, picomolar sensitivity
- Easy-to-use external filters
- Fluorescent labeling—no radioisotope usage
- Variable temperatures

Beacon™ 2000 Fluorescence Polarization System



The only single-tube FP instrument available, the compact Beacon™ 2000 fits right on your benchtop. Get the accuracy and convenience you need, but without the expense and hassle of complicated multiwell instruments.

Fluorescence polarization: real time, non-radioactive and sensitive measurement

An established, powerful tool, fluorescence polarization (FP) simplifies the study of molecular interactions in solution through the analysis of photonic emissions of fluorophore-tagged molecules in polarized light. By replacing tedious gel-shift assays, ELISAs, Western blots, and filter binding, FP streamlines research and saves

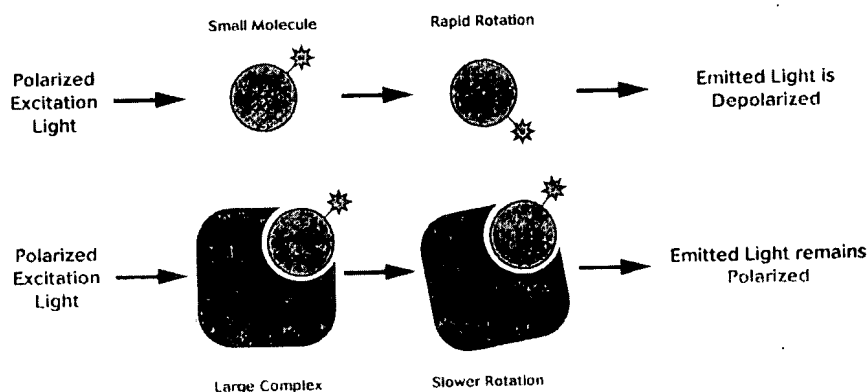
hours of time. It also delivers real time measurements, which are non-radioactive, sensitive, and homogenous. Common applications include the measurement of equilibrium binding, enzyme activity, protein degradation, and antibody affinity.

Fluorescence polarization made easy

The Beacon™ 2000 Fluorescence Polarization System adds convenience to the precision and speed of fluorescence polarization (Figure 1). Beacon™ 2000 FP System's compact size is perfect for a crowded work-

space, utilizing only a small footprint on your busy bench top. Its external-filter holders allow easy use of other fluorophores, while its standard disposable glass test tubes let you simply measure and go.

Figure 1 — Theory of fluorescence polarization



See the Invitrogen web site for an online version of the FP Applications Guide for more detail on FP theory and application:

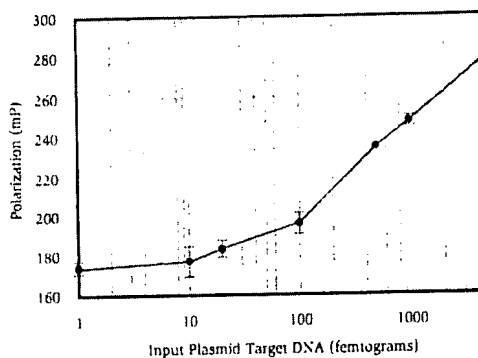
www.invitrogen.com/fpguide

Simple is better—and sensitive

The Beacon™ 2000 FP System's unique single-tube design is responsible for its efficient and practical proportions. It uses similar reagent volumes than its multiwell counterparts, it still maintains sensitivity to fluorescently labeled samples as small as 10 fmol/ml (Figure 2).

The target plasmid DNA was serially diluted from 5 picograms to 1.2 femtograms and each dilution was amplified by PCR in a 100 µl reaction. 80 µl of each amplification reaction were added to 10 µl of 1 N NaOH and incubated at 75°C for 30 minutes to denature the DNA. The 90 µl reactions were then added to 1 ml of 50mM Tris-HCl, 6X SSC, pH 8.0, at 37°C containing labeled oligos and blocking oligos. Hybridizations were incubated at 37°C for 30 minutes and then the FP values for each reaction were measured at 37°C on the Beacon™ 2000 System. The data represent the mean of triplicate experiments, \pm 1 standard deviation.

Figure 2 — Direct detection of hybridization between labeled oligos and PCR-amplified DNA

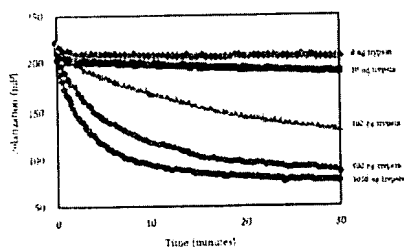


Quick and precise FP for many uses

Beacon™ 2000 FP System rapidly and accurately measures equilibrium binding and/or enzyme degradation in solution (Figure 3), with picomolar sensitivity, for a wide range of biological molecules. Useful in performing immunoassays, determining

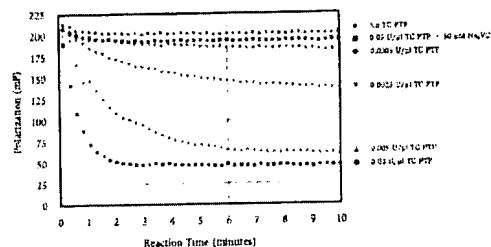
antibody specificity and affinity, it also measures protein-protein, protein-DNA, or receptor-ligand binding interactions. This system measures affinity binding directly in solution, with each data point obtained in a few seconds (Figure 4).

Figure 3 — FTC-Casein digestion with Trypsin



Trypsin was added to 1 ml 0.1 M Tris-HCl (pH 8.1). The reaction was started by addition of 5 pmoles FTC-casein. The fluorescence polarization was measured every 13 seconds on a Beacon™ 2000 instrument.

Figure 4 — Measuring phosphatase activity in real time



The enzymatic activity of T-Cell Protein Tyrosine Phosphatase (TC PTP) was measured in a dose-dependent manner by incubating different concentrations of TC PTP, which was from New England Biolabs (Beverly, MA). The TC PTP concentration ranged from 0.05 U/µl to 0.0005 U/µl. Each well also contained 50 µl of a mixture of anti-phosphotyrosine antibodies and fluorescein-labeled phosphopeptides in a final volume of 100 µl. Polarization values were measured continuously on a Beacon™ 2000 instrument after the addition of TC PTP (kinetic mode). Two control assays were performed; one did not receive TC PTP, while the other was supplemented with 50 µM of the potent phosphatase inhibitor Na_2VO_4 . In both cases, no dephosphorylation occurred and the polarization remained high throughout the experiment.

Put FP in your PC with Beacon™ 2000 Data Manager Software

The Beacon™ 2000 FP system can be used as a fully-functional stand-alone instrument. It comes equipped with onboard operating software specifically designed to enhance your research by allowing storage of up to 99 user-defined protocols. The Beacon™ 2000 FP system can also be used in concert with your PC, for even more powerful data acquisition. The included Beacon™ 2000 Data Manager Software enables the direct import of data recording and tabulation from the Beacon™

2000 instrument to your PC. The software presents the data in a form which is then easily copied and pasted into most popular spreadsheet programs*. The Data Manager software automatically displays and graphs data points in "real time" as they are acquired from the Beacon™ 2000 instrument. This feature allows you to easily monitor the progress of your experiment as it unfolds. You may also send data directly to a thermal paper printer (included).

*PC is not included. See page 6 for PC and spreadsheet specifications.

One instrument for one-stop FP

Don't waste your time shopping around. FP is just one-stop away. The Beacon™ 2000 FP system is fully functional instrument with all the accessories you need (Table 1).

Table 1 — Beacon™ 2000 System components

Beacon™ 2000 System components	
External Thermal Printer (parallel port, 40-column format)	
Complete Set of Starter Reagents including:	
One-Step FP Reference Kit (Cat. no. P3088)	
Protease Activity Detection Kit (Cat. no. PV2010)	
UV Standardization Kit (Cat. no. PV2500)*	
Beacon™ * 2000 Operator's Manual and FP Applications Guide	
Beacon™ 2000 Data Manager Software	
Required Computer Cables and Power Cords	
Fluorescein filters (490 nm excitation, 525 nm emission)	

*Included with the Red Range (Cat. no. P2810 and P2811) instruments.

Flexible format

There's a Beacon™ 2000 FP System that's right for you (Table 2). To meet your specific needs, this instrument comes in two formats: standard (360-700 nm) and red-range (254-900 nm).

Table 2 — Beacon™ 2000 catalog numbers

Beacon™ 2000 instrument	Wavelengths	Cat. no.
Standard 110 V instrument	360-700 nm	P2300
Red Range 110 V Instrument	254-900 nm	P2810
Standard 220 V instrument	360-700 nm	P2302
Red Range 220 V instrument	254-900 nm	P2811

The Beacon™ 2000 Fluorescence Polarization System—FP that fits

With the Beacon™ 2000 FP System, you get:

- Unique economical single-tube design
- Practical compact size
- Equilibrium binding directly in solution
- Fluorescent labeling eliminates use of radioisotopes
- Small sample volumes (100 µl)
- Variable temperature control (6-65°C)
- External filter holders—easy to use of other fluorophores
- Computer-controlled data collection
- Flexible instrument format
- Thermal printer for direct data acquisition

Start FP today

To learn how the Beacon™ 2000 Fluorescence Polarization System can accelerate your research, visit www.invitrogen.com (keyword: Beacon™).

Beacon™ 2000 Fluorescence Polarization Instrument Specifications

Highlights:

High Precision: Less than 2 mP standard deviation, at 1 nM fluorescein, for 0.1 ml sample.

High Sensitivity: Accurate to 10^{-11} M fluorescein in the polarization mode and 10^{-13} M fluorescein in the intensity mode, for 0.5 ml sample.

Variable Temperature Control: 6-65°C in 1°C increments, $\pm 1^\circ\text{C}$.

Sample Volumes and Standard Chamber: Sample volume 100 μl in disposable 6 mm x 50 mm glass test tubes.

Operating Software: Step-by-step prompting for measurement of blanks and samples.

Read Time: Static or Kinetic mode (minimum 6 seconds; number of read cycles variable, for very high precision.)

Programmable Protocols: Up to 99 user-defined protocols, password protected.

Output Signals and Printer: RS232 for interface with an IBM-compatible computer (not included); DB25 Parallel for interface with external parallel, thermal printer (included).

Data Manager Software: Microsoft® Windows® 3.1, 95, 98, NT, 2000, and XP compatible, graphical, data acquisition software provided for use on IBM-compatible computer (not included).

PC (not included) requirements for version 2.2b of the Beacon™ 2000 Data Manager Software:

Windows® 3.1, 95, 98 or NT, or Windows® 2000

Compatible Spreadsheet Programs

Microsoft® Excel, or Lotus 1-2-3, or into a plotting/curve-fitting program

Mechanical:

Sample Format: Single-tube

Overall Dimensions: 20.5" x 14.75" x 9.25" (52.6 cm x 37.8 cm x 23.7 cm)

Weight: 35 lb (15.9 kg)

Electro-Optical:

Excitation Illumination:

Standard Instrument: High-intensity 100 Watt quartz halogen lamp for 360-700 nm excitation.

Red-Range Instrument: Same as standard instrument plus 100 Watt high-intensity mercury lamp for excitation from 254-420 nm. Plus an enhanced photomultiplier tube that increases emission detection range to 900 nm.

Emission Detector: Photomultiplier tube (PMT) with selected high gain, low noise, low drift for 200-700 nm emission detection. An enhanced PMT that increases the emission detection range to 900 nm is also available in the Red-Range Instrument.

Optics: Six-element quartz optical system focuses excitation energy on the sample and collects focused, emitted fluorescent energy on the PMT detector. Excitation and emission polarizers and filters are in collimated light paths for optimum performance.

Optical Filters & Holders: Fluorescein filters standard, in easily accessible, external filter holders. Filter holders accommodate other wavelength filters for use with different fluorophores.

Polarizers:

Standard Instrument: Film polarizers.

Red-Range Instrument: Glan-Taylor type of prism polarizer.

Operating Environment:

Power: Two configurations: 110 V, 1.6 A @ 50 Hz, or 220-240 V, 2.0 A @ 50 Hz.

Operating Temperature: 15-25°C.

Related Products

The following products are available to use with the Beacon™ 2000 FP instrument. Please see www.invitrogen.com/drugdiscovery for updates to this list.

PolarScreen™ Fluorescence Polarization Assay Kits

Assay Description	Number of Assays†	Cat. no.
CDK Assay Kit, Rb ^{INC} , Green	100	P2928
CDK Assay Kit, Rb ^{INC} , Far Red	800 x 20 µl	PV3343
Protein Kinase C Assay Kit, Green	100	P2747
Protein Kinase C Assay Kit, Red	100	P2940
Protein Kinase C Assay Kit, Far Red	800 x 20 µl	PV3337
Ser/Thr Kinase Assay Kit, CREBride, Far Red	800 x 20 µl	PV3340
Ser/Thr Kinase Assay Kit, Crosstide, Green	100	P3103
Ser/Thr Kinase Assay Kit, Crosstide, Red	100	P3101
Ser/Thr Kinase Assay Kit, Crosstide, Far Red	800 x 20 µl	PV3331
Serine Kinase Assay Kit, IκB-α pSer32, Green	100	P2827
Serine Kinase Assay Kit, IκB-α pSer32, Far Red	800 x 20 µl	PV3334
Serine Kinase Assay Kit, IκB-α pSer36, Green	100	P2849
Threonine Kinase Assay Kit, PDK1, Green	100	P2884
Threonine Kinase Assay Kit, PDK1, Far Red	800 x 20 µl	PV3346
Tyrosine Kinase Assay Kit, Green	100	P2836
Tyrosine Kinase Assay Kit, Red	100	P2882
Tyrosine Kinase Assay Kit, Far Red	800 x 20 µl	PV3327
Androgen Receptor Assay Kit, Green	400 x 40 µl	P3018
Glucocorticoid Receptor Assay Kit, Green	100	P2816
Glucocorticoid Receptor Assay Kit, Red	100	P2893
Estrogen Receptor-alpha Assay Kit, Green	500	P2698
Estrogen Receptor-alpha Assay Kit, Red	400 x 40 µl	P3029
Estrogen Receptor-beta Assay Kit, Green	500	P2700
Estrogen Receptor-beta Assay Kit, Red	400 x 40 µl	P3032
Progesterone Receptor Assay Kit, Green	100	P2895
Progesterone Receptor Assay, Kit Red	100	P2962
PPARγ Assay Kit, Green	400 x 40 µl	PV3355
Estrogen Receptor-alpha Coactivator Assay Kit, Red	400 x 40 µl	P3071
Estrogen Receptor-beta Coactivator Assay Kit, Red	100	P2994
Protease Activity Detection Assay Kit		PV2010

†The volume of each assay is 100 µl unless otherwise indicated.

Microsoft and Windows are registered trademarks of Microsoft Corporation.
IBM and Lotus are registered trademarks of IBM Corporation.
GraphPad and Prism are trademarks of GraphPad Software.



These products may be covered by one or more Limited Use Label Licenses (See Invitrogen Catalog or www.invitrogen.com).
By use of these products you accept the terms and conditions of all applicable Limited Use Label Licenses.

For research use only. Not intended for any animal or human therapeutic or diagnostic use.
©2004 Invitrogen Corporation. All rights reserved. Reproduction forbidden without permission. Printed in the U.S.A.

Corporate headquarters:
1600 Faraday Avenue • Carlsbad, CA 92008 USA • Tel: 760 603 7200 • Fax: 760 602 6500 • Toll Free Tel: 800 955 6288 • E-mail: tech_service@invitrogen.com • www.invitrogen.com

European headquarters:
Invitrogen Ltd • Inchinnan Business Park • 3 Fountain Drive • Paisley PA4 9RF, UK • Tel: +44 (0) 141 814 6100 • Fax: +44 (0) 141 814 6260 • E-mail: eurotech@invitrogen.com

GraphPad Prism

5.0



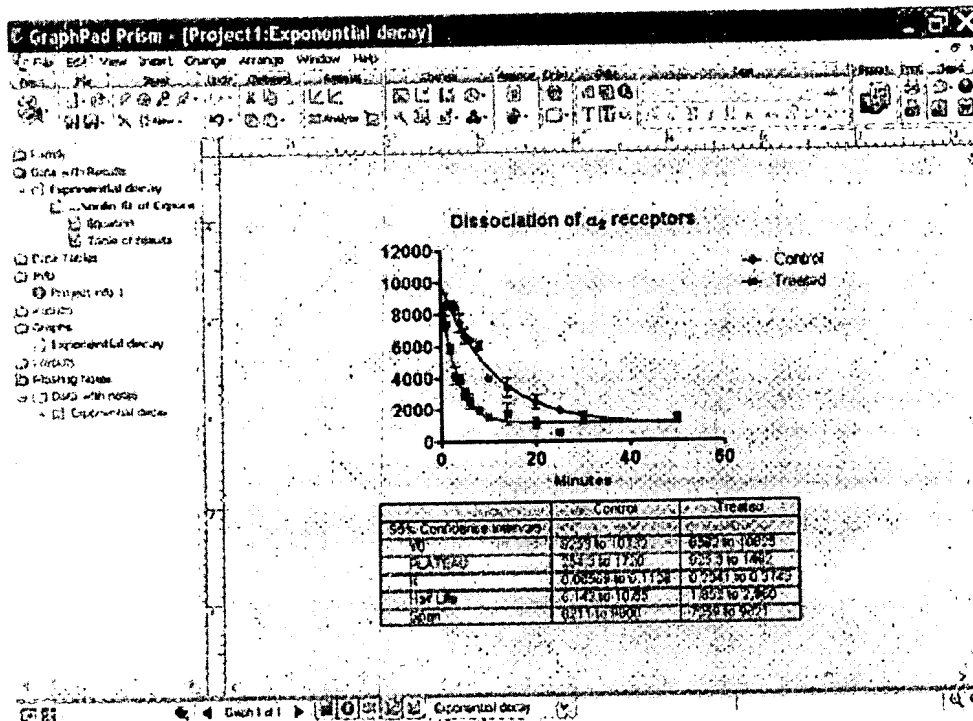
Learning Guide

Tour overview



What is GraphPad Prism?

GraphPad Prism is a powerful combination of biostatistics, curve fitting (nonlinear regression) and scientific graphing in one comprehensive program. This tour will highlight key features of the program and provide the basic training you'll need to get started. Use it as inspiration, not a rigid method. We've worked hard to make Prism easy and intuitive to use. Explore Prism yourself -- try things, make a few mistakes. If you get stuck, search this help file for tips and answers, about the [Prism program](#) itself, or about [statistical principles](#) you might not understand. We're sure you'll be up to speed in no time.



If you'd like to sit back and watch

If you prefer, you can watch an animated presentation of this tour. Launch Prism and from the Welcome dialog, select "Learn to use Prism."

Learn by doing -- Take a quick tour to learn the basics

In the next few pages, you'll get a quick tour of GraphPad Prism version 5. If you're new to Prism, it's a good way to get oriented. If you've used an earlier version of Prism, it is a great introduction to some of the new features.

[Learn how to begin a new project.](#)



The actin cytoskeleton-associated protein zyxin acts as a tumor suppressor in Ewing tumor cells

Valérie Amsellem^{a,*}, Marie-Hélène Kryszke^a, Martial Hervy^{a,1}, Frédéric Subra^a,
Rafika Athman^{b,2}, Hervé Leh^c, Corinne Brachet-Ducos^a, Christian Auclair^a

^aLaboratoire de Biotechnologie et Pharmacologie génétique appliquée, CNRS UMR 8113, Ecole Normale Supérieure de Cachan,
61 avenue du Président Wilson, 94230 Cachan, France

^bLaboratoire de Morphogénèse et Signalisation cellulaires, CNRS UMR 144, Institut Curie, 25 rue d'Ulm, 75005 Paris, France

^cBio Alliance Pharma, 59 boulevard du Général Martial Valin, 75015 Paris, France

Received 20 June 2004, revised version received 22 September 2004

Abstract

Changes in cell architecture, essentially linked to profound cytoskeleton rearrangements, are common features accompanying cell transformation. Supporting the involvement of the microfilament network in tumor cell behavior, several actin-binding proteins, including zyxin, a potential regulator of actin polymerization, may play a role in oncogenesis. In this work, we investigate the status of zyxin in Ewing tumors, a family of pediatric malignancies of bone and soft tissues, which are mainly associated with a t(11;22) chromosomal translocation encoding the EWS-FLI1 oncoprotein. We observe that EWS-FLI1-transformed murine fibroblasts, as well as human Ewing tumor-derived SK-N-MC cells, exhibit a complete disruption of their actin cytoskeleton, retaining very few stress fibers, focal adhesions and cell-to-cell contacts. We show that within these cells, zyxin is expressed at very low levels and remains diffusely distributed throughout the cytoplasm, instead of concentrating in actin-rich dynamic structures. We demonstrate that *zyxin* gene transfer into EWS-FLI1-transformed fibroblasts elicits reconstitution of zyxin-rich focal adhesions and intercellular junctions, dramatic reorganization of the actin cytoskeleton, decreased cell motility, inhibition of anchorage-independent growth and impairment of tumor formation in athymic mice. We observe similar phenotypic changes after *zyxin* gene transfer in SK-N-MC cells, suggesting that zyxin has tumor suppressor activity in Ewing tumor cells. © 2004 Elsevier Inc. All rights reserved.

Keywords. Actin cytoskeleton; Ewing tumor; EWS-FLI1; Zyxin

Introduction

In noncancer cells, adhesion to the extracellular matrix and to neighboring cells plays a central role in the control of cell survival, growth, differentiation and motility [1–3]. Upon oncogenic transformation, profound changes occur in cell

morphology and the organization of the cytoskeleton, in cell motility and in growth factor- or adhesion-dependent cell proliferation (for a review, see Ref. [4]). Disruption of the actin cytoskeleton and a concomitant reduction in the number of focal adhesions are common features accompanying cell transformation induced by various oncogenes. That the actin cytoskeleton plays a fundamental role in oncogenesis is suggested by the association of anchorage-independent growth and tumorigenicity with the rearrangements of the actin filament network observed in transformed cells [5]. Adhesive interactions involve specialized transmembrane receptors that are linked to the cytoskeleton through junctional plaque proteins (for a review, see Ref. [6]). The synthesis of several actin-binding proteins, including α -

* Corresponding author. CNRS UMR 8113, Institut Gustave Roussy, 39 rue Camille Desmoulins, 94805 Villejuif cedex, France. Fax: +33 1 4211 52 76.

E-mail address: vamsel@igr.fr (V. Amsellem).

¹ Present address: Huntsman Cancer Institute, Department of Biology, University of Utah, Salt Lake City, UT 84112, USA.

² Present address: Laboratoire d'Immunité innée et Signalisation, Institut Pasteur, Paris, France.

actinin, vinculin, tropomyosin and profilin, is down-regulated in transformed cells and overexpressing these proteins in tumor cells suppresses the transformed phenotype, which allows them to be considered as tumor suppressors.

Zyxin, a low abundance phosphoprotein, localizes to focal adhesions, to cell–cell contacts, along actin stress fibers and within the lamellipodia of migrating cells [7–9]. Zyxin directly interacts with α -actinin and Enabled/vasodilator-activated phosphoprotein (Ena/VASP), which connect it to actin filaments within these multicomponent structures. Anchoring of recombinant zyxin to the plasma membrane alters actin stress fiber organization within the cell. Artificial targeting of zyxin to the mitochondrion external membrane induces actin nucleation and polymerization at the surface of the organelle [10,11]. ActA, a protein encoded by the pathogenic bacterium *Listeria monocytogenes*, is highly homologous to zyxin and stimulates actin polymerization in vitro [10]. These observations suggest that zyxin, which colocalizes with actin-rich dynamic structures within the cell, may be implicated in the spatial control of actin filament assembly.

Zyxin expression is also deregulated in some cancer cells. It is overexpressed in acute myeloid leukemias [12], in melanomas [13] and upon fiber-induced carcinogenesis in rats [14]. Its synthesis is decreased in human fibroblasts transformed by simian virus 40, in bladder cancer cell lines and in several primary tumors [15,16]. Together with the actin cytoskeleton rearrangements commonly observed upon cell transformation, these properties of zyxin prompted us to investigate the status of the protein in a model of pediatric cancer, Ewing tumors, which are the second most common malignancies of bone arising in children and young adults. Ewing tumors are mainly associated with a t(11;22)(q24;q12) chromosomal translocation, encoding the chimerical transcription factor EWS-FLI1 [17,18]. Ectopic expression of EWS-FLI1 is sufficient to transform immortal murine fibroblasts [19–21], whereas inhibition of EWS-FLI1 expression in Ewing tumor-derived human cell lines, through antisense strategy or RNA interference, impairs anchorage-independent growth and in vivo tumorigenicity of the cells [22–24]. We show that zyxin levels are very low in EWS-FLI1-transformed NIH 3T3 fibroblasts and in the Ewing tumor-derived human cell line SK-N-MC, which exhibit a disorganized actin cytoskeleton. We demonstrate that zyxin gene transfer into these cells contributes to the suppression of their transformed phenotype, suggesting that zyxin down-regulation may participate in EWS-FLI1-induced oncogenesis.

Materials and methods

Cell culture

The NIH 3T3 cell line (3T3) was purchased from ATCC. The EWS-FLI1-transformed NIH 3T3 cell line (3T3-EF)

was a kind gift from J. Ghysdael (Orsay, France). These cells are 3T3 fibroblasts that have been stably transduced by the cDNA encoding the type 1 EWS-FLI1 fusion protein inserted downstream of the Mo-MuLV long terminal repeat in the pBabe-puro retroviral vector. All the 3T3-derived cell lines are cultured in Dulbecco's modified Eagle's medium (DMEM) supplemented with 100 UI/ml penicillin, 100 μ g/ml streptomycin and 10% heat-inactivated newborn calf serum (all from Gibco). 3T3-EF-derived cells are selected with 2.5 μ g/ml puromycin (Sigma). FlyA13 is an amphotropic packaging cell line used to encapsidate the pLNCX retroviral shuttle, in which the Mo-MuLV Gag-Pol and RD114 Env functions are encoded by two distinct plasmids [25]. FlyA13 cells (gift from F.L. Cosset, Lyon, France) are grown in DMEM supplemented with 100 UI/ml penicillin, 100 μ g/ml streptomycin and 10% heat-inactivated fetal calf serum (all from Gibco), plus 4 μ g/ml blasticidin and 10 μ g/ml phleomycin (Cayla). The SK-N-MC cell line was purchased from ATCC. It is a human Ewing tumor-derived cell line harboring a type 1 EWS-FLI1 fusion gene. This cell line is cultured in Eagle's minimum essential medium supplemented with 100 UI/ml penicillin, 100 μ g/ml streptomycin, 0.1 mM nonessential amino acids and 10% heat-inactivated fetal calf serum (all from Gibco). Cells stably transduced with pLNCX- or pcDNA3-derived expression vectors are selected with G418 (Gibco) at 0.8 (3T3-derived cell lines) or 0.25 mg/ml (SK-N-MC-derived cell lines).

Plasmid constructs

The full-length cDNA encoding human zyxin was excised from the pZyxinGFP plasmid (a kind gift from M. C. Beckerle, Salt Lake City, UT) through *Bam*HI–*Hind*III restriction and inserted between the *Bgl*II and *Hind*III sites of the pLNCX vector (Clontech), downstream of the human cytomegalovirus (CMV) immediate early promoter/enhancer. A sequence encoding three flag peptides was added, in the same reading frame, downstream of the zyxin coding sequence, through *Avr*II–*Nsi*I restriction. The resulting construct was called pLNCX-zyxin. The CMV promoter in pLNCX or pLNCX-zyxin was replaced by the EF1 α promoter through *Bam*HI–*Sal*I restriction. Then the EF1 α or EF1 α -zyxin sequence was substituted to the CMV promoter in the pcDNA3.1 vector (Invitrogen) through *Nru*I–*Xba*I restriction to generate pcDNA3-EF1 α and pcDNA3-EF1 α -zyxin, respectively.

Cell transfection and infection

The FlyA13 packaging cell line was transfected with the pLNCX or the pLNCX-zyxin vector (0.15 μ g/cm²) using Superfect reagent (Qiagen) following manufacturer's instructions. Cells expressing the *neo*^R gene were selected for 7 days with 0.8 mg/ml G418, pooled, expanded and plated into 75-cm² flasks at a density of 25,000 cells/cm² for

viral particle production. Two days later, the culture medium was replaced by DMEM without G418. On the third day, the virus-containing medium was harvested, filtered through a 0.45- μ m pore size membrane, aliquoted and frozen. Virus titers were determined by infection of 3T3 fibroblasts. Infection of 3T3 and 3T3-EF cells in zyxin reexpression experiments was performed at a multiplicity of infection of 0.1. After 1 week, infected cells were selected with G418 and amplified as polyclonal populations of cells stably transduced by pLNCX (3T3-control and 3T3-EF-control) or pLNCX-zyxin (3T3-zyxin and 3T3-EF-zyxin). SK-N-MC cells were transfected with the pcDNA3-EF1 α and pcDNA3-EF1 α -zyxin vectors by calcium phosphate coprecipitation, using 50 μ g DNA per 50-cm² dish. G418 was added 24 h later. Cells stably transduced with pcDNA3-EF1 α and pcDNA3-EF1 α -zyxin were grown as polyclonal populations (SK-N-MC-control and SK-N-MC-zyxin).

Western blot

Total proteins were extracted from cells at 70% confluence with ice-cold RIPA (10 mM Tris-HCl, pH 7.4, 100 mM NaCl, 1 mM EDTA, 1% Triton X-100, 0.5% Na deoxycholate, 0.1% SDS) in the presence of Complete™ protease inhibitor mix (Roche). After incubation for 30 min at 4°C, samples were centrifuged for 10 min at 14,000 rpm. Supernatants were collected and protein concentrations were measured by the Bradford assay (Biorad). Eighty micrograms of proteins were boiled in Laemmli buffer and electrophoresed on a 10% SDS-polyacrylamide gel according to standard procedures. The proteins were electroblotted onto a Hybond C-Extra membrane (Amersham) in 20 mM sodium phosphate, pH 6.7. The membrane was blocked by 10% powder milk in TBST (20 mM Tris-HCl, pH 7.5, 500 mM NaCl, 0.1% Tween 20) for 1 h at room temperature. Incubation with the primary antibody (164D4 mouse anti-zyxin antibody provided by J. Wehland, Braunschweig, Germany, mouse anti-flag M2 antibody, Sigma, or mouse anti- α -tubulin antibody, Santa Cruz) was carried out overnight at 4°C in TBST. Incubation with an anti-mouse IgG secondary antibody, conjugated to alkaline phosphatase (Biorad), was carried out for 1 h at room temperature. Detection was performed by enhanced chemiluminescence (Immun-Star, Biorad). Quantification of the signals on the films was achieved with the Bioprofil BioID software.

Fluorescent staining

Cells were seeded onto glass cover slips at a density of 2000 cells/cm². Seventy-two hours later, cells were fixed for 20 min in PBS containing 3% paraformaldehyde. The paraformaldehyde solution was neutralized with 50 mM NH₄Cl. Extraction was carried out for 4 min with 0.4% Triton X-100 in PBS. Cells were incubated for 1 h with blocking buffer (3% bovine serum albumin in PBS) and then for 1 h with undiluted 164D4 anti-zyxin antibody, M2

anti-flag antibody (2 μ g/ml, Sigma) or phalloidin-FITC (265 nM, Sigma) in blocking buffer. Cells treated with anti-zyxin or anti-flag antibody were then incubated with a donkey anti-mouse IgG antibody conjugated to TRITC (Jackson ImmunoResearch) for 30 min at room temperature. Cover slips were mounted in Vectashield™ (Zymed) and observed through a fluorescence microscope (Nikon).

Cell motility

For wound migration assays, cells were grown to confluence in 60-mm dishes. A wound was introduced in the monolayer with a sharp, 1-mm-thick plastic scraper. Twenty-four hours later, cells were observed by phase contrast light microscopy. For video recording, cells were seeded onto glass cover slips at 20% confluence 72 h before recording. Cover slips were incubated in hermetic mini-chambers at 37°C in a humidified 5% CO₂ atmosphere (Leica). Phase contrast photographs were taken every 4 min for 20 h with a video recorder (Leica). The movements of the cells were analyzed with the Metamorph software (Universal Imaging, Downingtown, PA) allowing to reconstitute the track of each cell and to measure its length.

In vitro clonogenicity assay

Cells were embedded in complete culture medium supplemented with 0.8% methylcellulose (Methocel MC4000, Sigma), seeded in triplicate into 35-mm dishes and incubated at 37°C in a humidified 5% CO₂ atmosphere. The number of cells seeded was 1000 cells per dish for 3T3-derived cell lines and 5000 cells per dish for SK-N-MC-derived cell lines. After 4 weeks, macroscopic clones (diameter > 120 μ m) were counted.

In vivo tumorigenicity assay

Eight female nude mice, aged 6–8 weeks, were inoculated with each cell line tested. Animals were housed in sterile, air-conditioned atmosphere, given food and water in standard conditions and handled in a sterile laminar-flow hood. The mice were irradiated at 5 Gy the day before injection. Subcutaneous injection was performed with 10⁶ mouse cells or 5 \times 10⁶ human cells in 0.2 ml PBS. Tumor development was monitored once a week. The length (L) and width (W) of each tumor were measured to calculate tumor volume (V) as follows: $V = 2W(L/2)^2$.

Results

Zyxin expression is down-regulated in EWS-FLI1-transformed 3T3 fibroblasts

In order to investigate the status of zyxin in EWS-FLI1-transformed cells, we used murine 3T3 fibroblasts that have

been transduced with the pBabe-puro retroviral vector designed for expression of the EWS-FLI1-encoding cDNA under the control of the CMV promoter. When compared to the parental 3T3 fibroblasts, EWS-FLI1-expressing cells display a more rounded shape, with fewer cytoplasmic extensions and a reduced spreading area. They establish no stable cell-to-cell contacts. Their morphological characteristics and their behavior in culture remind those of transformed cells, in agreement with previously published studies on immortal murine fibroblasts ectopically expressing EWS-FLI1 (e.g., Ref. [20]). To explore possible correlations between cell morphology and cytoskeleton organization, we performed actin filament staining with phalloidin-FITC on parental (3T3) and EWS-FLI1-expressing (3T3-EF) NIH 3T3 fibroblasts. 3T3 cells exhibit a highly organized actin filament network comprised of numerous, thick stress fibers (Fig. 1a) whereas the actin cytoskeleton is entirely disrupted in 3T3-EF cells, showing no stress fibers at all. Actin remains diffusely distributed within the cytoplasm or accumulates into lamellipodia (Fig. 1j). The overall level of actin is the same in the two cell types (data not shown). We then proceeded with zyxin immunostaining in these cells. In 3T3 fibroblasts, zyxin is found in association with stress fibers, focal adhesions, the cell edge and cell-to-cell contacts (Fig. 1b). In 3T3-EF cells, zyxin staining is faint. The protein is no longer found associated with any particular cytoskeletal structure, cell-to-matrix, or cell-to-cell contacts. Some zyxin is present in the lamellipodia (Fig. 1k). To see whether poor staining of zyxin in 3T3-EF cells is due to down-regulation of its expression in the presence of EWS-FLI1, we analyzed total protein extracts from 3T3 and 3T3-EF cells by Western blotting. We observed that zyxin is underexpressed in EWS-FLI1-transformed cells (Fig. 2A, lane 4), as compared with parental, 3T3 fibroblasts (Fig. 2A, lane 1). Zyxin levels were quantified in three independent Western blot experiments using the Bioprofil Bio1D software. As shown in Fig. 2B (compare 3T3-EF to 3T3), the level of zyxin is reduced by 50–75% upon 3T3 cell transformation by EWS-FLI1. Zyxin expression is not reduced when 3T3 fibroblasts are transduced with the empty pBabe-puro control vector (data not shown). Our results demonstrate that disruption of the actin cytoskeleton correlates with reduced expression of zyxin in 3T3 fibroblasts transformed by EWS-FLI1.

Reexpression of zyxin in EWS-FLI1-transformed 3T3 fibroblasts

In order to explore the contribution of zyxin down-regulation to the tumoral phenotype, we decided to reexpress the protein in EWS-FLI1-transformed 3T3 fibroblasts. For this purpose, the cDNA encoding human zyxin, fused to a C-terminal flag, was inserted downstream of the CMV promoter in the pLNCX shuttle vector to generate the pLNCX-zyxin plasmid, and recombinant retroviral particles were prepared to infect 3T3-EF cells. As a control, infection

was performed with viral particles derived from the pLNCX empty vector. In both cases, transduced cell populations (3T3-EF-zyxin and 3T3-EF-control) were selected with G418. Zyxin expression was monitored by Western blot analysis using the 164D4 anti-zyxin monoclonal antibody. Endogenous zyxin is detected at very low levels in 3T3-EF, 3T3-EF-control and 3T3-EF-zyxin cells (mouse zyxin: Fig. 2A, lanes 4–6). Human zyxin can be detected in 3T3-EF-zyxin cells (flagged human zyxin: Fig. 2A, lane 6). Note that the flagged human protein migrates slower than the native murine protein in SDS-PAGE, allowing for distinction between endogenous and exogenous zyxin in transduced cells. The level of zyxin reached in 3T3-EF-zyxin cells exceeds by 1.5- to 2-fold, that of endogenous zyxin in parental 3T3 fibroblasts (Fig. 2A, compare lane 6 to lane 1), as confirmed by the results of total zyxin quantification (Fig. 2B). We verified that an anti-flag antibody allowing for the detection of exogenous human zyxin in 3T3-EF-zyxin cells does not cross-react with the endogenous mouse zyxin (Fig. 2C). Before going on and studying the effects of zyxin reexpression on the phenotype of the transformed fibroblasts, we have checked the levels of EWS-FLI1 in 3T3-EF, 3T3-EF-control and 3T3-EF-zyxin cells and found that these remain identical in the three cell lines (data not shown).

Zyxin reexpression induces morphological changes and cytoskeleton reorganization in EWS-FLI1-transformed fibroblasts

We began the phenotypic characterization of the 3T3-EF-zyxin cell line by light microscopic observations and by actin and zyxin fluorescent staining. Reexpression of zyxin in 3T3-EF cells alters their morphology and behavior in culture. Transduced cells recover a flat morphology resembling that of parental 3T3 fibroblasts, display extended spreading areas and make large cell–cell contacts. Actin staining of these cells demonstrates that such morphological changes are supported by a major reorganization of their cytoskeleton: numerous actin filament bundles are observed throughout the cytoplasm of the 3T3-EF-zyxin cells, reminding the stress fibers seen within parental fibroblasts, albeit somewhat shorter and thinner than the original structures (Fig. 1p). Furthermore, immunostaining of the cells with the anti-zyxin antibody shows that, upon reexpression in 3T3-EF cells, zyxin no longer appears diffusely distributed throughout the cytoplasm but relocates to the length and ends of actin bundles, to the cell edge, to focal adhesions and intercellular junctions (Fig. 1q). Immunostaining of the cells with the anti-flag antibody gives identical results, revealing that exogenous human zyxin has the same subcellular distribution in 3T3-EF-zyxin cells as mouse endogenous zyxin in parental 3T3 fibroblasts (Fig. 1r). 3T3-EF-control cells transduced by the pLNCX empty vector exhibit the same morphology, actin cytoskeleton architecture and zyxin localization as 3T3-EF fibroblasts (Figs. 1m, n, o).

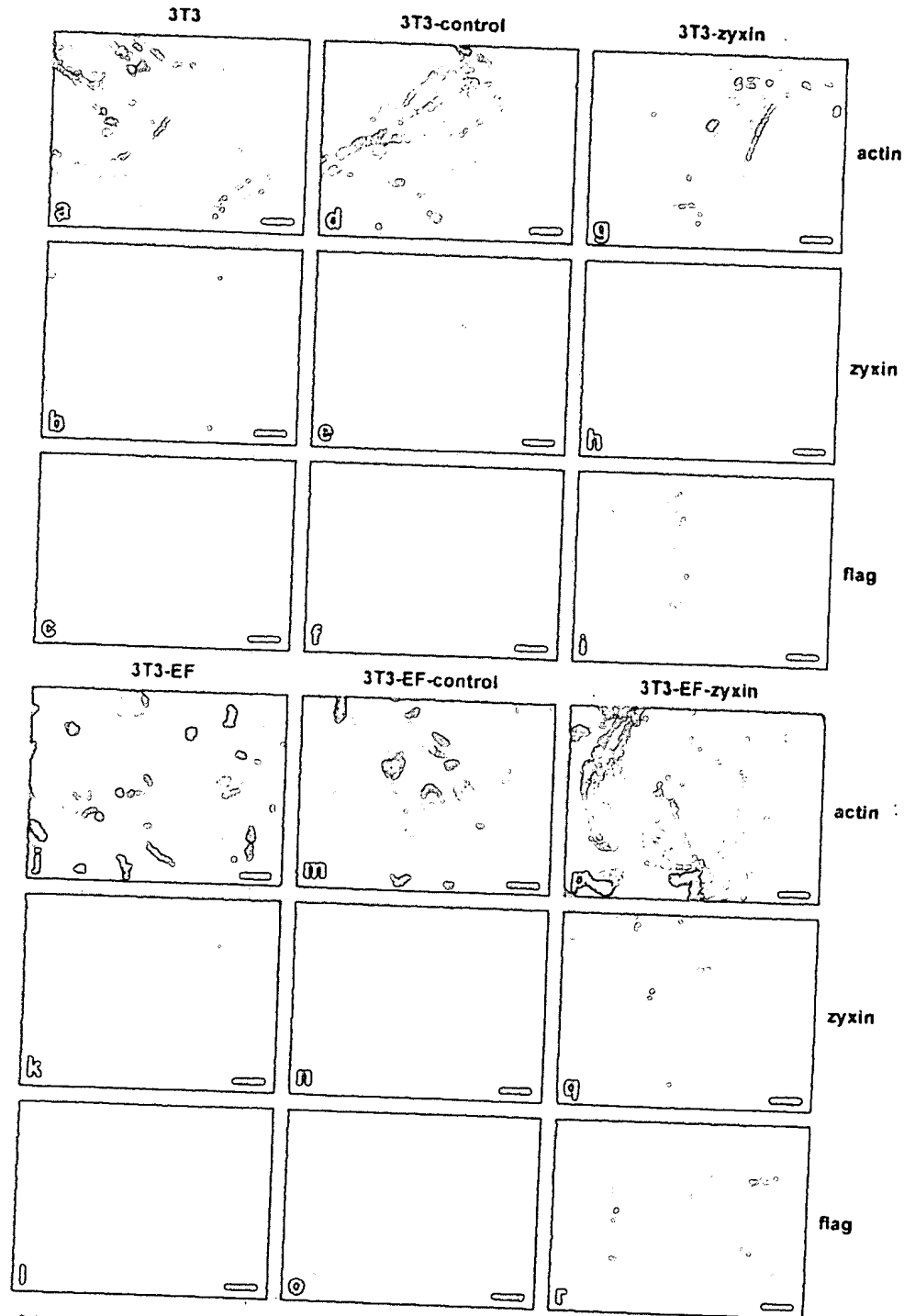


Fig. 1. Architecture of the actin cytoskeleton and subcellular distribution of zyxin in parental and EWS-FLI1-transformed NIH 3T3 fibroblasts—effects of zyxin reexpression. Six cell lines were analyzed by fluorescence microscopy: 3T3 (a–c), 3T3-control (d–f), 3T3-zyxin (g–i), 3T3-EF (j–l), 3T3-EF-control (m–o) and 3T3-EF-zyxin (p–r), after staining of actin by phalloidin-FITC (a, d, g, j, m, p), of total zyxin by the 164D4 monoclonal antibody (b, e, h, k, n, q) or of exogenous zyxin by the M2 anti-flag monoclonal antibody (c, f, i, l, o, r). Anti-zyxin and anti-flag antibodies were revealed by a TRITC-conjugated anti-mouse IgG antibody. Scale bar = 20 μ m.

Because the total level of zyxin in 3T3-EF-zyxin cells is higher than in parental 3T3 cells, we checked for the effects that zyxin overexpression could exert in nontransformed cells. We infected parental 3T3 fibroblasts with retroviral

particles derived from the zyxin-encoding pLNCX plasmid or the empty pLNCX vector to produce two G418-resistant cell populations, the 3T3-zyxin and 3T3-control cell lines, respectively. Western blot analysis shows that the endoge-

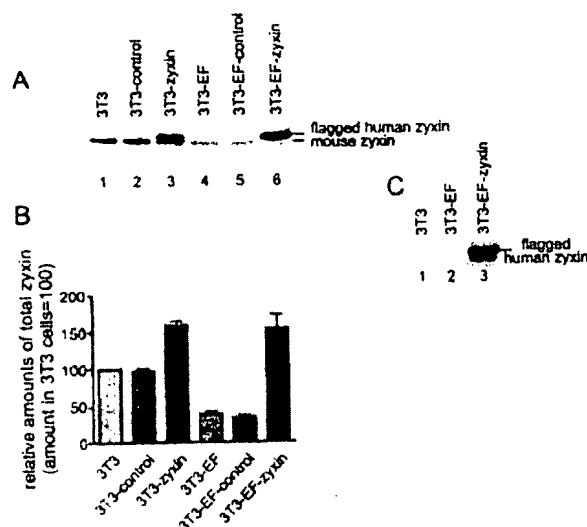


Fig. 2. Western blot analysis of zyxin expression in 3T3- and 3T3-EF-derived cells. (A) Zyxin expression detected with the 164D4 monoclonal antibody in uninfected 3T3 (lane 1) and 3T3-EF cells (lane 4), in 3T3 and 3T3-EF cells infected with control pLNCX vector (3T3-control, lane 2; 3T3-EF-control, lane 5) or with the zyxin-encoding vector (3T3-zyxin, lane 3; 3T3-EF-zyxin, lane 6). (B) Relative amounts of total zyxin (endogenous plus exogenous) in the six cell lines analyzed. Three independent Western blot experiments were performed and the amounts of zyxin were quantified with the Bioprofil BioID software. Graph represents mean values \pm SEM. (C) Western blot demonstrating the specificity of the M2 anti-flag monoclonal antibody towards exogenous zyxin, which is present in 3T3-EF-zyxin (lane 3) but not in 3T3 (lane 1) or 3T3-EF cells (lane 2).

nous levels of zyxin are unaltered in the transduced cells (Fig. 2A, lanes 1–3, mouse zyxin) and that the levels of exogenous zyxin obtained in 3T3-zyxin cells (Fig. 2A, lane 3, flagged human zyxin) are similar to those obtained in 3T3-EF-zyxin cells (Fig. 2A, lane 6, flagged human zyxin). These observations are confirmed by quantitative analysis (Fig. 2B). No changes in cell morphology, actin cytoskeleton organization or zyxin distribution were observed in the 3T3-control cell line (Fig. 1, compare d, e, f to a, b, c) and in the 3T3-zyxin cell line (Fig. 1, compare g, h to a, b). Again, the exogenous zyxin (Fig. 1i) has the same subcellular localization as the endogenous zyxin (Figs. 1i and b). All these observations lead to the conclusion that zyxin reexpression in 3T3-EF cells specifically suppresses the effects of EWS-FLI1-induced transformation on cell morphology, actin filament organization and zyxin subcellular distribution.

Zyxin reexpression reduces the intrinsic motility of EWS-FLI1-transformed fibroblasts

Because cytoskeletal organization and actin polymerization play crucial roles in cell migration, which is involved in tumor progression and invasion, we then wanted to know whether zyxin reexpression in EWS-FLI1-transformed fibroblasts would affect the intrinsic motility of the cells. To get an overall evaluation of their motile properties, we

first compared the behavior of 3T3-EF-zyxin cells to that of 3T3-EF cells in a wound healing assay. Cells were grown to confluence and a wound was created in the cell layer with a plastic scraper. Migration of the cells beyond the border of the wound, into the empty space, was monitored 24 h later. Photographs are shown for 3T3, 3T3-EF, 3T3-EF-control and 3T3-EF-zyxin cells, as well as for the 3T3-control and 3T3-zyxin cell lines (Fig. 3). We observe that 3T3 fibroblasts show minimal individual cell migration into the wound (Fig. 3a). On the contrary, 3T3-EF cells migrate beyond the border of the wound into its whole area (Fig. 3d) and the same result is obtained with the 3T3-EF-control cell line (Fig. 3e). The behavior of the 3T3-EF-zyxin cells in this assay is intermediate between that of 3T3 and that of 3T3-EF cells: a significant number of cells migrate beyond the border of the wound, but the central part of the empty area remains devoid of cells (Fig. 3f). Transduction with the pLNCX control vector or overexpression of zyxin does not change the behavior of parental 3T3 fibroblasts: minimal individual cell migration into the wound is observed with 3T3-control and 3T3-zyxin cells (Figs. 3b and c). Thus, EWS-FLI1-induced transformation of 3T3 fibroblasts results in increased cell motility, whereas zyxin reexpression in the EWS-FLI1-transformed fibroblasts results in reduced cell motility.

To get further insight into the behavior of 3T3-EF and 3T3-EF-zyxin cells, we then performed video recordings of their migration on the surface of glass cover slips. For this purpose, two clones, 3T3-EF-zyxin1 and 3T3-EF-zyxin2, were isolated from the 3T3-EF-zyxin cell population. Zyxin reexpression was confirmed in these two clones by Western blotting as shown in Fig. 4C. These clones were cultured within incubation chambers on a phase-contrast microscope. Cell movements were recorded for 20 h with a numerical

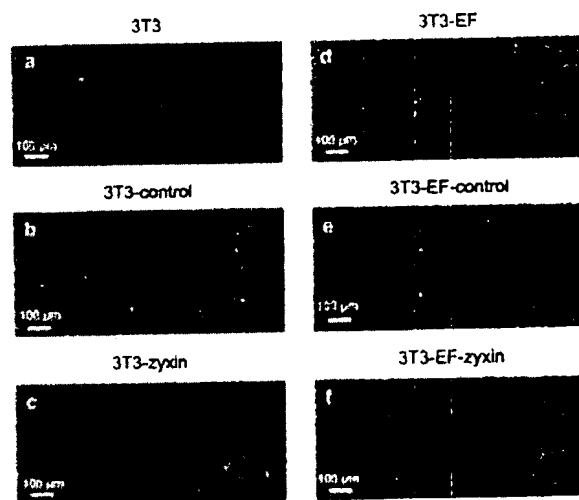


Fig. 3. Wound healing assay performed on 3T3- and 3T3-EF-derived cell lines. Phase contrast photographs of 3T3 (a), 3T3-control (b), 3T3-zyxin (c), 3T3-EF (d), 3T3-EF-control (e) and 3T3-EF-zyxin cells (f) after 24 h of cell migration into a 1-mm wound at the surface of 60-mm tissue culture dishes. Scale bar = 100 µm.

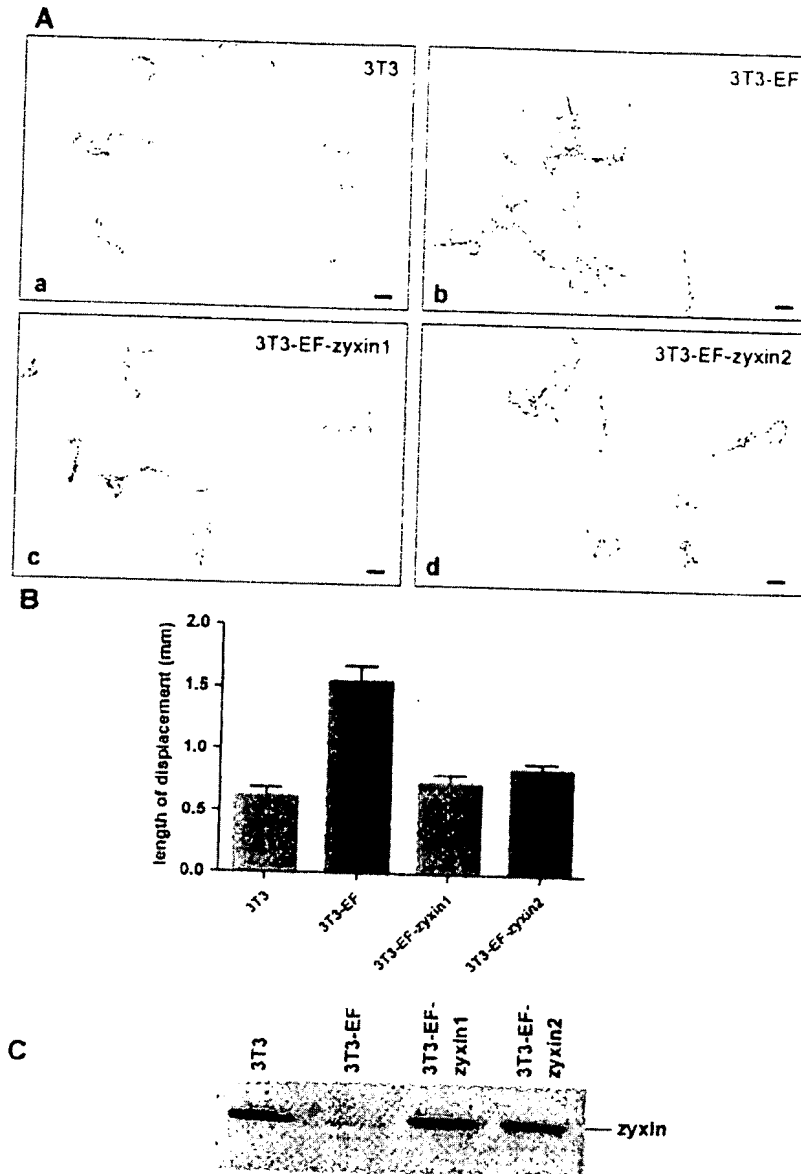


Fig. 4. Intrinsic motility of 3T3, 3T3-EF and 3T3-EF-zyxin cells at the surface of glass cover slips. (A) Four cell lines were analyzed by video recording for a period of 20 h: parental 3T3 fibroblasts (a), EWS-FLI1-transformed 3T3 cells (b) and two clones of 3T3-EF cells transduced with the human *zyxin* gene, 3T3-EF-zyxin1 (c) and 3T3-EF-zyxin2 (d). Each line represents the track of an individual cell. Scale bar = 10 μ m. (B) The length of each track was measured and the mean of the values obtained for each cell line was plotted on a bar graph \pm SEM. (C) Control Western blot showing the levels of total zyxin expressed in each cell line.

camera and analyzed with the Metamorph software. The results were compared to those obtained with the 3T3 and 3T3-EF cell lines. The tracks of a dozen of cells are drawn in Fig. 4A for 3T3, 3T3-EF, 3T3-EF-zyxin1 and 3T3-EF-zyxin2 fibroblasts. The length of each track was measured and the mean of the values obtained with each cell line for a 20-h migration was plotted on a bar graph (Fig. 4B). These experiments show that the mean distance covered by the cells in 20 h is 0.6 mm for 3T3 cells and 1.5 mm for 3T3-EF cells. The values obtained with 3T3-EF-zyxin1 and 3T3-EF-zyxin2 cells are 0.7 and 0.8 mm, respectively. The differences observed between 3T3-EF and 3T3 cells on the one

hand, and between each of the 3T3-EF-zyxin clones and 3T3-EF cells on the other hand, are significant (Student's *t* test: $P < 0.0001$). Because we infer that differences in cell motility depend on the relative levels of zyxin initially expressed in the cell lines studied, we verified by Western blot that these levels do not vary with cell density (not shown), in agreement with the results of previous studies performed on migrating keratinocytes [26]. Supporting the conclusions drawn from the wound healing assay, as can be seen on the video record available online (supplementary data), changes in the migratory behavior of the cells can be attributed to two phenomena. First, the movement of 3T3-

EF cells on the surface of the cover slips occurs at higher speed than the movement of 3T3 or 3T3-EF-zyxin cells. Second, 3T3 and 3T3-EF-zyxin cells exhibit a high propensity to establish strong and stable intercellular junctions when they come into contact with each other, which impedes their migration, shortening their mean displacement around twofold.

Reexpression of zyxin suppresses anchorage-independent growth and tumorigenicity of EWS-FLI1-transformed fibroblasts

Among the properties acquired by transformed cells is anchorage-independent growth, which reflects the ability of the cells to proliferate in the absence of signaling from the extracellular matrix. This characteristic can be assessed through evaluation of cell clonogenicity in semisolid medium. Thousand cells were seeded per 35-mm dish in culture medium supplemented with methylcellulose. Clones with a diameter larger than 120 μm were counted after 4 weeks. Each cell line was tested in triplicate and the mean number of clones per dish was plotted on a bar graph (Fig. 5). Parental 3T3 fibroblasts are unable to grow in semisolid medium. In the same conditions, 3T3-EF cells give rise to the growth of 264 clones per dish. With the 3T3-EF-zyxin cell line, only 28 clones per dish are obtained, whereas 3T3-EF-control cells grow as well as the 3T3-EF cells (280 clones per dish). The reduction in clonogenicity between 3T3-EF (or 3T3-EF-control) and 3T3-EF-zyxin cells is significant ($P < 0.0001$). Overexpression of zyxin in 3T3 cells or transduction of these cells with the empty pLNCX vector (3T3-control cell line) does not affect their behavior in semisolid medium: no clones are obtained with these two cell lines. Thus, reexpression of zyxin in EWS-FLI1-transformed fibroblasts strongly and specifically reduces their anchorage-independent growth capacity.

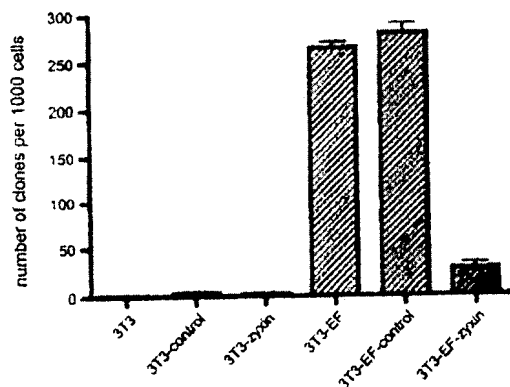


Fig. 5. Anchorage-independent growth of 3T3- and 3T3-EF-derived cells assayed in methylcellulose-supplemented medium. For each of the cell lines tested (3T3, 3T3-control, 3T3-zyxin, 3T3-EF, 3T3-EF-control and 3T3-EF-zyxin), 1000 cells were seeded per 35-mm dish in complete growth medium supplemented with 0.8% methylcellulose. Colonies $>120 \mu\text{m}$ were counted after 4 weeks. Bar graph represents the means \pm SEM of the values obtained in three dishes for each cell line.

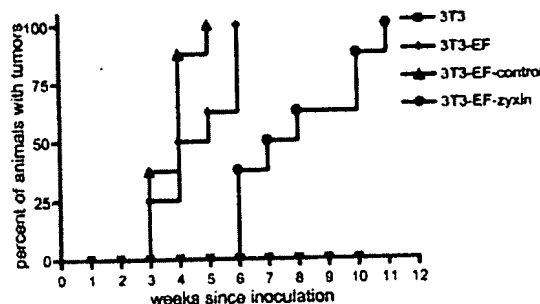


Fig. 6. In vivo tumorigenicity of 3T3, 3T3-EF, 3T3-EF-control and 3T3-EF-zyxin cells. Tumor formation was monitored after subcutaneous injection of 10^6 cells in nude mice. Percent of animals that have developed a tumor is plotted against time and statistical significance is evaluated by the log rank test. P values are calculated with respect to the results obtained with the 3T3-EF cell line.

In order to see whether the loss of in vitro clonogenicity correlates with reduced tumorigenicity in vivo, tumor formation was assessed in nude mice after subcutaneous inoculation of 3T3, 3T3-EF and 3T3-EF-zyxin cells. For each cell line, the time separating cell inoculation from tumor detection was recorded in eight mice. Statistical significance was evaluated with the log rank test (Fig. 6). No tumor formed after inoculation of parental 3T3 cells. Tumors appeared between 3 and 6 weeks for 3T3-EF and 3T3-EF-control cells, with a median time of 4 weeks. For 3T3-EF-zyxin cells, tumors appeared between six and 11 weeks, with a median time of 7.5 weeks. This result significantly differs from that obtained with 3T3-EF and 3T3-EF-control cells ($P < 0.0001$). In agreement with the impairment of anchorage-independent growth in vitro observed upon zyxin reexpression in EWS-FLI1-transformed fibroblasts, tumorigenicity of 3T3-EF-zyxin cells in nude mice is significantly reduced as compared to that of 3T3-EF cells.

Effects of zyxin overexpression in the Ewing tumor-derived human cell line SK-N-MC

The human cell line SK-N-MC was established from a Ewing tumor expressing the type 1 EWS-FLI1 fusion. To check the level of expression of zyxin in this cell line, we performed Western blot experiments. Since the histological origin of Ewing tumors is unknown, no healthy counterpart of the tumor cells is available for comparative studies. However, comparing zyxin expression levels in 3T3, 3T3-EF and SK-N-MC cells, we observe that the level of zyxin protein in the human cell line, as revealed with the 164D4 antibody, seems to be as low as in 3T3-EF cells (Fig. 7, lanes 1 to 3). Thus, we decided to overexpress zyxin in SK-N-MC cells and to analyze the effects of exogenous zyxin on the phenotype of these cells. SK-N-MC cells were stably transfected with the pcDNA3-EF1 α -zyxin plasmid, which encodes human zyxin harboring a C-terminal flag, or with the pcDNA3-EF1 α empty vector. G418-resistant cell populations were selected, generating the SK-N-MC-zyxin and SK-N-MC-control cell lines, respectively. Zyxin is

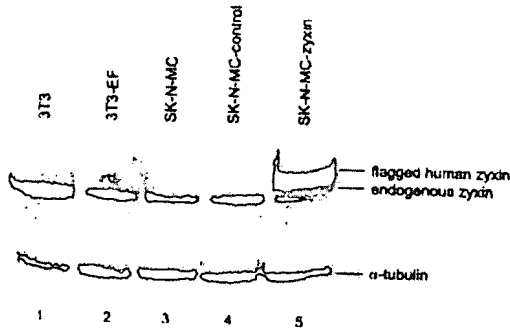


Fig. 7. Western blot analysis of zyxin expression in murine and human EWS-FLI1-transformed cells. Total zyxin (endogenous and exogenous) was detected with the 164D4 monoclonal antibody (upper panel) in 3T3 (lane 1) and 3T3-EF (lane 2) murine fibroblasts and in the Ewing tumor-derived human cell line SK-N-MC, either untransfected (lane 3), stably transfected with the empty pcDNA3.1 vector (SK-N-MC-control, lane 4) or stably transfected with the zyxin-encoding pcDNA3.1 vector (SK-N-MC-zyxin, lane 5). Loading control was performed on the same blot with an anti- α -tubulin mouse monoclonal antibody (lower panel).

detected in whole cell extracts from these two populations by Western blot (Fig. 7, upper panel). Exogenous zyxin can be distinguished from endogenous zyxin on the blots due to the presence of the flag, which slows its migration. Thus, exogenous zyxin is expressed at a level similar to that of the endogenous zyxin present in 3T3 fibroblasts (Fig. 7, compare lane 5, flagged human zyxin, to lane 1, endogenous zyxin), whereas the level of endogenous zyxin remains unchanged upon transfection of the SK-N-MC cells with the pcDNA3-EF1 α -zyxin plasmid or with the pcDNA3-EF1 α empty vector (Fig. 7, lanes 3–5, endogenous zyxin). Loading control was performed on the same blot with an anti- α -tubulin monoclonal antibody (Fig. 7, lower panel).

SK-N-MC cells grow as dense clusters of small cells. Fluorescent staining of actin and zyxin in these cells shows that the actin cytoskeleton is entirely destructured and that zyxin is of low abundance with a diffuse distribution throughout the cytoplasm (Figs. 8a, b). The SK-N-MC-

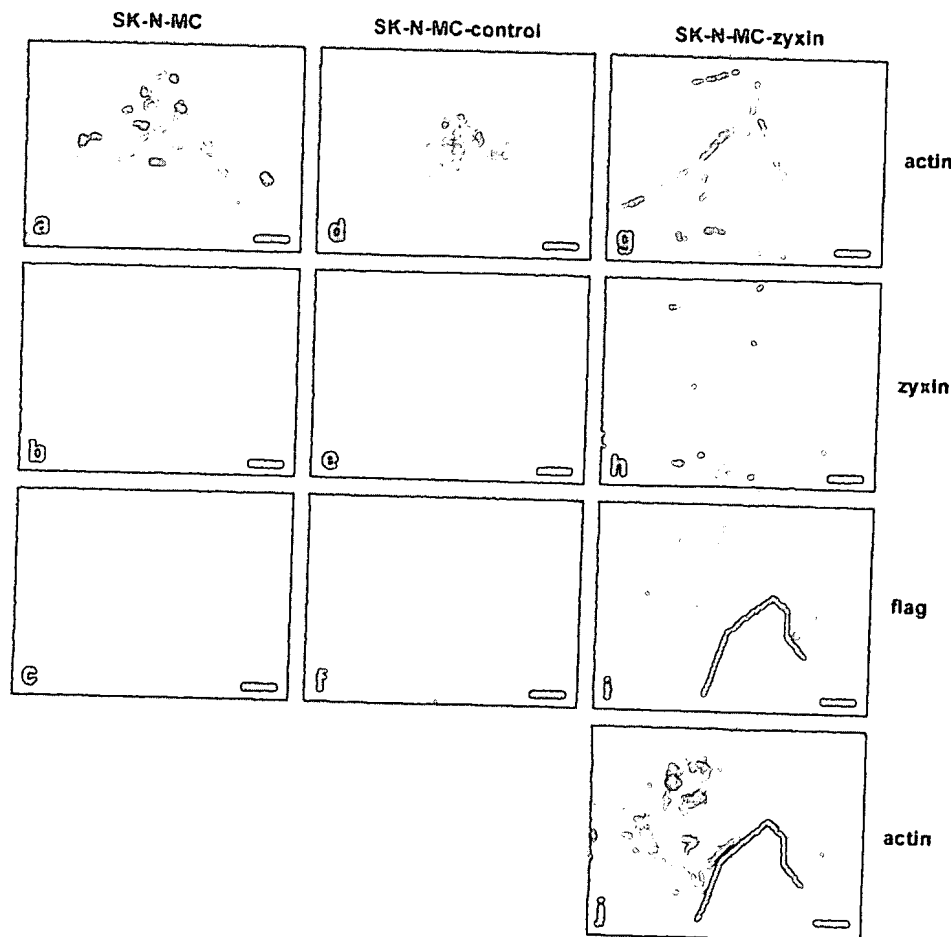


Fig. 8. Architecture of the actin cytoskeleton and subcellular distribution of zyxin in the SK-N-MC Ewing tumor-derived human cell line—effects of zyxin overexpression. Three cell lines were analyzed by fluorescence microscopy: SK-N-MC (a–c), SK-N-MC-control (d–f), SK-N-MC-zyxin (g–i), after staining of actin by phalloidin-FITC (a, d, g, j), of total zyxin by the 164D4 monoclonal antibody (b, e, h) or of exogenous zyxin by the M2 anti-flag monoclonal antibody (c, f, i). Anti-zyxin and anti-flag antibodies were revealed by a TRITC-conjugated anti-mouse IgG antibody. Scale bar = 20 μ m.

zyxin cell population includes cells that display a considerable increase in their spreading area, long thick actin stress fibers, and punctate zyxin-rich structures at the border of the cells and within intercellular junctions (Figs. 8g, h). Transfection of SK-N-MC cells with the empty pcDNA3-EF1 α vector does not affect cell morphology or cytoskeletal organization (Figs. 8d, e). In SK-N-MC-zyxin cells, staining of zyxin with the anti-flag antibody demonstrates that the subcellular localization of exogenous and total zyxin is the same (Fig. 8, compare i and h). Furthermore, since the pcDNA3-EF1 α -zyxin-transfected cell population is heterogeneous, we can observe that cells that display a flat morphology, associated with the presence of actin stress fibers, express detectable levels of exogenous zyxin, which concentrates along the cell border or within cell-to-cell contacts (see cells immediately above white line in Figs. 8i and j), whereas cells that do not express exogenous zyxin retain their small size and disorganized actin cytoskeleton (see cells below white line in Figs. 8h and i). We conclude that zyxin overexpression correlates with actin network reorganization and cell spreading in Ewing tumor-derived human SK-N-MC cells.

In order to know whether zyxin overexpression in SK-N-MC cells affects their tumoral phenotype, we tested the ability of SK-N-MC-zyxin to grow in semisolid medium. For each of the SK-N-MC, SK-N-MC-control and SK-N-MC-zyxin cell lines, three 35-mm dishes were seeded with 5000 cells embedded in culture medium supplemented with methylcellulose. Clonogenicity was checked after 4 weeks and the mean number of clones (>120 μ m) per dish was plotted in a bar graph (Fig. 9). SK-N-MC and SK-N-MC-control cells gave rise to 284 and 290 clones per dish,

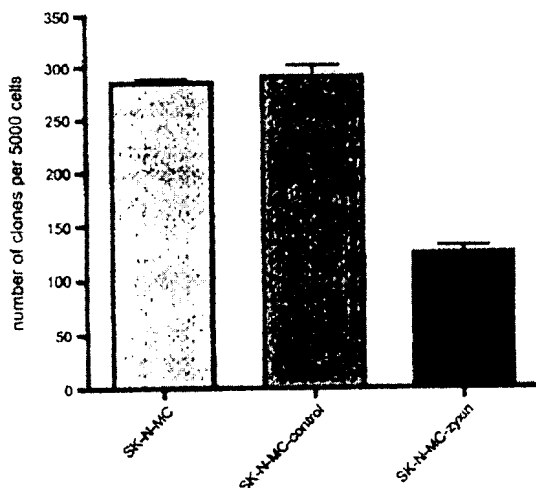


Fig. 9 Anchorage-independent growth of SK-N-MC-derived cells assayed in methylcellulose-supplemented medium. For each of the three cell lines tested (SK-N-MC, SK-N-MC-control, SK-N-MC-zyxin), 5000 cells were seeded per 35-mm dish in complete growth medium supplemented with 0.8% methylcellulose. Colonies >120 μ m were counted after 4 weeks. Bar graph represents the means \pm SEM of the values obtained in three dishes for each cell line.

respectively. Only 124 clones were obtained with the SK-N-MC-zyxin cells. With this test, the effect of zyxin overexpression in SK-N-MC cells is not so clearcut as in 3T3-EF cells. This may be due to heterogeneity in exogenous zyxin expression within the population of transduced human tumor cells, which is not observed in the EWS-FLI1-transformed murine fibroblasts. However, the reduction in the number of clones obtained is significant ($P < 0.0001$), allowing us to conclude that zyxin overexpression impairs anchorage-independent growth of SK-N-MC cells.

Although the effects of zyxin gene transfer appear to be less dramatic in SK-N-MC cells than in 3T3-EF cells, we were interested in checking for the in vivo tumorigenicity of SK-N-MC-zyxin cells as compared to that of SK-N-MC and SK-N-MC-control cells. The behavior of SK-N-MC-derived cells differs from that of 3T3-EF-derived cells after injection into nude mice. First, a higher number of SK-N-MC cells has to be inoculated for tumor development to occur (5×10^6 instead of 10^6 cells). Second, tumors appear earlier: all the animals inoculated with SK-N-MC-derived cells develop tumors within one to 2 weeks following injection. Third, tumors grow very fast, so that the experiment had to be interrupted at 6 weeks post-injection because tumor volume was too high in control mice to go on. In these assay conditions, we observe that zyxin overexpression in SK-N-MC cells does not delay tumor formation in nude mice but that it reduces the rate of tumor growth. Tumors induced by SK-N-MC-zyxin cells appear at the same time as tumors induced by SK-N-MC or SK-N-MC-control cells. However, as shown in Fig. 10, 6 weeks after inoculation, the mean tumor volume is lower for SK-N-MC-zyxin cells (587 mm³) than for SK-N-MC cells (2433 mm³) or SK-N-MC-control cells (2819 mm³). Student's *t* test analysis of these results indicates that the values obtained with SK-N-MC and SK-N-MC-control cells are not significantly different from each other, but significantly differ from those obtained with SK-N-MC-zyxin cells ($P < 0.05$). Thus, in vivo tumorigenicity assay in nude mice shows that an inhibitory effect on tumor progression is elicited upon zyxin overexpression in SK-N-MC cells.

Discussion

A number of indirect observations led us to study the contribution of zyxin to the tumoral phenotype in EWS-FLI1-transformed cells: (i) malignant transformation alters cell morphology, cytoskeletal architecture, adhesion and motility [4]; (ii) zyxin associates with specialized actin structures and is implicated in the regulation of cytoskeleton architecture and dynamics [7–9]; (iii) zyxin expression is deregulated upon transformation of several cell lines [13–15]. Because the histogenic origin of Ewing tumors is still unknown, no healthy counterpart of Ewing tumor cells is

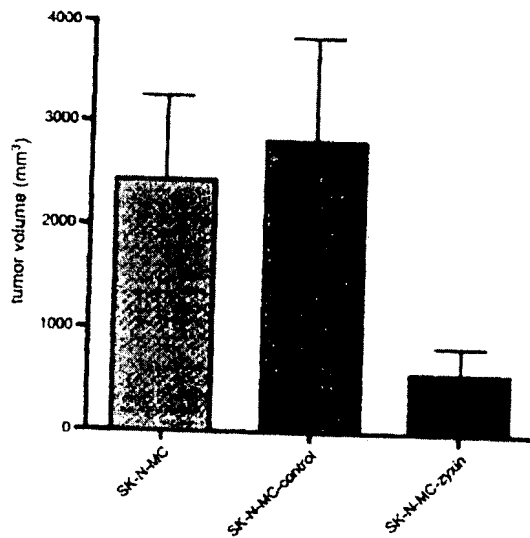


Fig. 10. In vivo tumorigenicity of SK-N-MC, SK-N-MC-control and SK-N-MC-zyxin cells. Tumor formation was monitored after subcutaneous injection of 5×10^6 cells in nude mice. Average tumor volume is reported 6 weeks after injection. Bar graph represents the means \pm SEM of the values obtained in eight mice for each cell line.

available for comparative studies. Two hypotheses have essentially been retained: Ewing tumors would either derive from neuroectodermal or from mesenchymal precursors. Diverse models have been used to try and elucidate the mechanisms of EWS-FLI1-induced oncogenesis. Among them, immortal mouse fibroblasts can be considered as a useful experimental support, since they are the only cells that can be thoroughly transformed by EWS-FLI1 and they seemed to us particularly well-designed to analyze the changes in cytoskeleton architecture accompanying cell transformation in a mesenchymal cellular background. We actually observe that upon transformation by EWS-FLI1, 3T3 fibroblasts lose their flat morphology, their actin cytoskeleton is disorganized, they acquire high motility, anchorage-independent growth and tumorigenicity in nude mice. Zyxin expression is reduced in the transformed cells as compared with the parental fibroblasts. Zyxin gene transfer into these cells restores the levels of zyxin protein characteristic of normal cells, and thereupon, the transformed phenotype is at least partially reverted: cells with higher levels of zyxin recover a fibroblastic morphology, stress fibers, focal adhesions and cell-to-cell contacts; they exhibit reduced intrinsic motility, anchorage-independent growth and tumorigenicity in nude mice. Our experiments were carried out with polyclonal cell populations, thereby excluding a possible influence of vector integration site on cell phenotype. We observe that human zyxin efficiently reverts the effects of murine zyxin underexpression in 3T3 fibroblasts. Human and mouse zyxin are highly homologous proteins and ectopic human zyxin exhibits the same subcellular distribution after gene transfer in 3T3-EF cells as the endogenous mouse zyxin in parental fibroblasts, suggesting that both proteins are functionally indistinguish-

able. Although our results do not allow us to draw any conclusion about the role of zyxin loss in the etiology of Ewing tumors in human, reversion of the tumoral phenotype induced by zyxin gene transfer in murine fibroblasts is validated in a human Ewing tumor-derived cell line: in SK-N-MC cells, which also produce low constitutive levels of zyxin, overexpression of the protein similarly tends to suppress the transformed phenotype, as indicated by microscopic observations, in vitro anchorage-independent growth and in vivo tumorigenicity assays. In this way, zyxin exhibits some of the properties of a tumor suppressor. Of course, it will be interesting in the near future to see whether changes in zyxin protein levels can also be detected in the diverse models used to study EWS-FLI1-induced modulation of gene expression, such as EWS-FLI1-transduced murine marrow stromal cells [27] or human neuroblastoma cells [28].

Transient inhibition of zyxin expression has been achieved in 3T3 fibroblasts using the siRNA technology, which results in a loss of stress fibers and focal adhesions, without affecting cell viability and growth [29]. These results are in agreement with our observations, since we show that zyxin underexpression in EWS-FLI1-transformed 3T3 fibroblasts is associated with similar cytoarchitecture alterations. Furthermore, zyxin reexpression in 3T3-EF cells does not affect cell proliferation (data not shown). That no other changes related to cell transformation occur in siRNA-treated cells may be due to the fact that only transient effects have been studied in this system. Also, disruption of the zyxin-encoding gene in knockout mice does not affect the viability, fertility or tissue architecture of the animals [30]. Similar results have been obtained when two other potential tumor suppressor genes, *gelsolin* and *VASP*, were disrupted: knockout mice displayed a viable phenotype and did not develop spontaneous cancers, although some alterations in cell adhesion and migration could be observed [31,32]. The absence of zyxin at the beginning of life may be compensated through the activation of alternate pathways during development, whereas the loss of zyxin in differentiated cells may not.

The mechanism by which zyxin suppresses tumorigenicity is not clear. Zyxin acts as a molecular scaffold to facilitate the assembly of multiprotein complexes that promote actin polymerization at specific sites within the cell. Important partners of zyxin in this function are α -actinin and Ena/VASP. In epithelial cells, disrupting zyxin- α -actinin interaction leads to the mislocalization of zyxin and Ena-VASP, which is accompanied by disturbances in actin filament assembly and by changes in cell morphology [33]. Increasing zyxin levels in transformed cells could promote the cooperative assembly of focal adhesion proteins such as α -actinin, vinculin and talin, shifting the equilibrium between the soluble and membrane-bound pools of these molecules, to form stable cell-matrix contacts. Stabilization of these structures would favor adhesion and inhibit motility, thereby reducing tumorigenicity. In agreement

with this hypothesis, other actin-binding proteins included in adhesion plaques are underexpressed in transformed cells and reversion of the tumoral phenotype is induced by overexpression of these proteins in cancer cells, as demonstrated for α -actinin in SV40-transformed 3T3 fibroblasts and in human malignant neuroblastoma [34,35]. In adherent fibroblasts, actin stress fibers are anchored to focal adhesions and intercellular junctions, two types of cell structure where zyxin concentrates. Transformed cells that have lost their actin stress fibers display fewer focal adhesions and intercellular junctions [36,37]. This is true for 3T3-EF cells, where zyxin is less abundant than in parental cells and remains diffusely distributed within the entire cytoplasm. When zyxin is reexpressed in 3T3-EF cells, actin stress fibers reappear, together with zyxin-containing focal adhesions and cell–cell contacts, suggesting that zyxin may contribute to the stabilization of the actin cytoskeleton and the adherent structures of the cell. Because α -actinin binds to zyxin and has been shown to interact with β 1-integrin [38], this protein would contribute to the cross-linking of zyxin and the actin cytoskeleton to transmembrane integrins within focal adhesions. Mutual stabilization of stress fibers and focal adhesions probably occurs owing to both actin filament bundling within the cytoplasm and integrin clustering at the cell surface in response to the binding of extracellular matrix components. Integrins participate in cell signaling, transducing cell proliferation signals from the extracellular matrix into the cytoplasm. Disruption of this integrin-dependent signaling pathway in transformed cells results in anchorage-independent growth, which appears, in our experiments, to be suppressed by zyxin. Also, α -actinin cross-links zyxin to cadherins through α - and β -catenins at epithelial cell-to-cell junctions [39]. The fact that cadherin underexpression is often observed in cancer cells [40] suggests that intercellular junctions play an important role in tumor suppression, which may require the presence of zyxin in these structures. In NIH 3T3 fibroblasts, we have detected the presence of β -catenin within intercellular junctions (results not shown). In these cells, homotypic cell–cell adhesion has been reported to be essentially mediated by N-cadherin [41]. Together with the observations made after zyxin immunostaining of 3T3 and 3T3-EF-zyxin cells (Figs. 1b, q), these data suggest that zyxin may participate in the stabilization of intercellular junctions in 3T3 fibroblasts.

How zyxin function may be related to cell motility is also an open question. Our observations on EWS-FLI1-transformed 3T3 fibroblasts indicate that zyxin underexpression correlates with increased cell motility. During migration of an adherent fibroblast, polarized actin polymerization at the leading edge of the cell pushes the plasma membrane forward, thereby sustaining the extension of filopodia and progression of the lamellipodium. The membrane protrusion becomes anchored to the substratum through adhesion complexes. Actin filament bundles contract within the body of the cell, while actin depolymerization takes place at the

rear of the cell [42]. The migration process thus requires a highly organized actin network, a tight control of actin polymerization and depolymerization, and a rapid turnover of cell–matrix adhesion structures. In EWS-FLI1-transformed 3T3 fibroblasts, actin-rich lamellipodia are observed, where actin polymerization may be controlled by the recruitment of Ena/VASP: actually, it was demonstrated that, although VASP interacts with zyxin and localizes to the tips of lamellipodia in migrating fibroblasts, zyxin does not colocalize with VASP in these dynamic structures and is not required for the proper localization of VASP in the lamellipodium [43]. Zyxin is also absent from the adhesion complexes assembled during cell migration, where actin dynamics is controlled by paxillin. However, at the end of the migration, when the leading edge stops and retracts, zyxin accumulates within cell–matrix contacts that mature into large, stable focal adhesions contributing to cell spreading [44]. We hypothesize that the low levels of zyxin available in EWS-FLI1-transformed cells would not impair actin polymerization in the lamellipodium but would be insufficient to allow for focal adhesion and cell–cell contact stabilization, thus favoring increased motility.

Some of the tumor-suppressing properties of zyxin might also be independent of its physical interaction with the actin cytoskeleton. The C-terminal region of zyxin is comprised of three LIM domains that interact with members of the CRP family of cysteine-rich proteins and with hWarts/LATS1 [45,46]. CRP2 is dramatically underexpressed in avian fibroblasts transformed by retroviral oncogenes or chemical carcinogens [47], which suggests that zyxin-dependent impairment of CRP functions might be associated with cell transformation. The tumor suppressor hWarts/LATS1 is a serine threonine kinase that interacts with a Cdc2-phosphorylated form of zyxin on the mitotic apparatus in dividing cells. When this interaction is disrupted, cells fail to exit from mitosis, which leads to chromosomal instability, a hallmark of malignant tumors [46]. Cerisano et al. [48] showed that zyxin expression is up-regulated in response to CD99 in the 6647 Ewing tumor-derived cell line and that siRNA-mediated inhibition of zyxin synthesis impairs CD99-induced apoptosis in these cells. This observation further argues in favor of potential tumor suppressor functions for zyxin, in this case relying upon its involvement in a proapoptotic signaling pathway. Finally, because zyxin shuttles between the nucleus and sites of adhesion in fibroblasts, it might relay information from the cell surface to the nuclear compartment to regulate the transcriptional apparatus [49], a hypothesis supported by the finding that physical association between zyxin and the E6 protein of the human papillomavirus type 6 results in the accumulation of zyxin in the nucleus where it can function as a transcriptional activator [50]. Zyxin-induced reversion of the transformed phenotype in Ewing tumor cells may also involve modulation of gene expression.

By way of a conclusion, zyxin may act as a tumor suppressor in cancer cells with low endogenous expression

levels of this protein. The gene encoding zyxin maps at 7q32, a chromosomal region that is affected in a variety of human cancers. 7q monosomy or partial deletion of this chromosome arm is frequently found in myelodysplastic syndrome, acute myeloid, juvenile myelomonocytic and acute lymphocytic leukemias, as well as in breast carcinoma [51,52]. In some of these malignancies, chromosome mapping has identified the 7q31–35 region as commonly involved in the rearrangements [52–54]. The significance of this association may rely on the presence of a previously undescribed tumor suppressor gene in this region and the zyxin gene may be the candidate.

Acknowledgments

We thank J. Ghysdael for the gift of the 3T3-EF cell line, F.L. Cosset for the gift of the FlyA13 cell line, M.C. Beckerle for the zyxin cDNA and J. Wehland for the 164D4 anti-zyxin antibody. We thank P. Ardouin and co-workers at the Gustave Roussy Institute for assistance in in vivo tumorigenicity experiments. This work was supported by the Centre National de la Recherche Scientifique, the French Ministry of Education and Research and a grant from the Ligue contre le Cancer to V. Amsellem.

References

- [1] K.A. Beningo, M. Dembo, I. Kaverina, J.V. Small, Y.L. Wang, Nascent focal adhesions are responsible for the generation of strong propulsive forces in migrating fibroblasts, *J. Cell Biol.* 153 (2001) 881–888.
- [2] S.M. Frisch, R.A. Screaton, Anoikis mechanisms, *Curr. Opin. Cell Biol.* 13 (2001) 555–562.
- [3] F.M. Watt, Role of integrins in regulating epidermal adhesion, growth and differentiation, *EMBO J.* 21 (2002) 3919–3926.
- [4] G. Pawlak, D.M. Helfman, Cytoskeletal changes in cell transformation and tumorigenesis, *Curr. Opin. Genet. Dev.* 11 (2001) 41–47.
- [5] P. Kahn, D. Heller, S. Shin, Structural correlates of cellular tumorigenicity and anchorage independence in transformed fibroblasts, *Cytogenet. Cell Genet.* 36 (1983) 605–611.
- [6] Nagafuchi, Molecular architecture of adherens junctions, *Curr. Opin. Cell Biol.* 13 (2001) 600–603.
- [7] M.C. Beckerle, Identification of a new protein localized at sites of cell–substrate adhesion, *J. Cell Biol.* 103 (1986) 1679–1687.
- [8] A.W. Crawford, M.C. Beckerle, Purification and characterization of zyxin, an 82,000-dalton component of adherens junctions, *J. Biol. Chem.* 266 (1991) 5847–5853.
- [9] R.M. Golsteyn, D. Louvard, E. Friederich, The role of actin binding proteins in epithelial morphogenesis: models based upon *Listeria* movement, *Biophys. Chem.* 68 (1997) 73–82.
- [10] R.M. Golsteyn, M.C. Beckerle, T. Koay, E. Friederich, Structural and functional similarities between the human cytoskeletal protein zyxin and the ActA protein of *Listeria monocytogenes*, *J. Cell Sci.* 110 (1997) 1893–1906.
- [11] J. Fradelizi, V. Noireaux, J. Plastino, B. Menichi, D. Louvard, C. Sykes, R.M. Golsteyn, E. Friederich, ActA and human zyxin harbour Arp2/3-independent actin-polymerization activity, *Nat. Cell Biol.* 3 (2001) 699–707.
- [12] T.R. Golub, D.K. Slonim, P. Tamayo, C. Huard, M. Gaasenbeek, J.P. Mesirov, H. Coller, M.L. Loh, J.R. Downing, M.A. Caligiuri, C.D. Bloomfield, E.S. Lander, Molecular classification of cancer: class discovery and class prediction by gene expression monitoring, *Science* 286 (1999) 531–537.
- [13] E.J. van der Gaag, M.T. Leccia, S.K. Dekker, N.L. Jalbert, D.M. Amodeo, H.R. Byers, Role of zyxin in differential cell spreading and proliferation of melanoma cells and melanocytes, *J. Invest. Dermatol.* 118 (2002) 246–254.
- [14] H. Sandhu, W. Dehnen, M. Roller, J. Abel, K. Unfried, mRNA expression patterns in different stages of asbestos-induced carcinogenesis in rats, *Carcinogenesis* 21 (2000) 1023–1029.
- [15] J. Zumbunn, B. Trueb, A zyxin-related protein whose synthesis is reduced in virally transformed fibroblasts, *Eur. J. Biochem.* 241 (1996) 657–663.
- [16] M. Sanchez-Carbajo, N.D. Socci, E. Charytonowicz, M. Lu, M. Prystowsky, G. Childs, C. Cordon-Cardo, Molecular profiling of bladder cancer using cDNA microarrays: defining histogenesis and biological phenotypes, *Cancer Res.* 62 (2002) 6973–6980.
- [17] O. Delattre, J. Zucman, B. Plougastel, C. Desmaza, T. Melot, M. Peter, H. Kovar, I. Joubert, P. de Jong, G. Rouleau, A. Aurias, G. Thomas, Gene fusion with an ETS DNA-binding domain caused by chromosome translocation in human tumours, *Nature* 359 (1992) 162–165.
- [18] W.A. May, S.L. Lessnick, B.S. Braun, M. Klemsz, B.C. Lewis, L.B. Lunsford, R. Hromas, C.T. Denny, The Ewing's sarcoma EWS/FLI-1 fusion gene encodes a more potent transcriptional activator and is a more powerful transforming gene than FLI-1, *Mol. Cell. Biol.* 13 (1993) 7393–7398.
- [19] S.L. Lessnick, B.S. Braun, C.T. Denny, W.A. May, Multiple domains mediate transformation by the Ewing's sarcoma EWS/FLI-1 fusion gene, *Oncogene* 10 (1995) 423–431.
- [20] Y. Song, R.S. Maul, C.S. Gerbin, D.D. Chang, Inhibition of anchorage-independent growth of transformed NIH3T3 cells by epithelial protein lost in neoplasm (EPLIN) requires localization of EPLIN to actin cytoskeleton, *Mol. Biol. Cell* 13 (2002) 1408–1416.
- [21] D. Chan, T.J. Wilson, D. Xu, H.E. Cowdery, E. Sanij, P.J. Hertzog, I. Kola, Transformation induced by Ewing's sarcoma associated EWS/FLI-1 is suppressed by KRAB/FLI-1, *Br. J. Cancer* 88 (2003) 137–145.
- [22] M. Ouchida, T. Ohno, Y. Fujimura, V.N. Rao, E.S. Reddy, Loss of tumorigenicity of Ewing's sarcoma cells expressing antisense RNA to EWS-fusion transcripts, *Oncogene* 11 (1995) 1049–1054.
- [23] G. Lambert, J.R. Bertrand, E. Fataf, F. Subra, H. Pinto-Alphandary, C. Malvy, C. Auclair, P. Couvreur, EWS fl-1 antisense nanocapsules inhibits Ewing sarcoma-related tumor in mice, *Biochem. Biophys. Res. Commun.* 279 (2000) 401–406.
- [24] T. Dohjima, N.S. Lee, H. Li, T. Ohno, J.J. Rossi, Small interfering RNAs expressed from a Pol III promoter suppress the EWS/FLI-1 transcript in an Ewing sarcoma cell line, *Molec. Ther.* 7 (2003) 811–816.
- [25] F.L. Cosset, Y. Takeuchi, J.L. Battini, R.A. Weiss, M.K. Collins, High-titer packaging cells producing recombinant retroviruses resistant to human serum, *J. Virol.* 69 (1995) 7430–7436.
- [26] M.T. Leccia, E.J. van der Gaag, N.L. Jalbert, H.R. Byers, Zyxin redistributes without upregulation in migrating human keratinocytes during wound healing, *J. Invest. Dermatol.* 113 (1999) 651–657.
- [27] E.C. Torchia, S. Jaishankar, S.J. Baker, Ewing tumor fusion proteins block the differentiation of pluripotent marrow stromal cell, *Cancer Res.* 63 (2003) 3464–3468.
- [28] C.J. Rorie, V.D. Thomas, P. Chen, H.H. Pierce, J.P. O'Bryan, B.E. Weissman, The Ews/Fl-1 fusion gene switches the differentiation program of neuroblastomas to Ewing sarcoma/peripheral primitive neuroectodermal tumors, *Cancer Res.* 64 (2004) 1266–1277.
- [29] J. Harborth, S.M. Elbashir, K. Bechert, T. Tuschl, K. Weber, Identification of essential genes in cultured mammalian cells using small interfering RNAs, *J. Cell Sci.* 114 (2001) 4557–4565.

- [30] L.M. Hoffman, D.A. Nix, B. Benson, R. Boot-Hanford, E. Gustafsson, C. Jamora, A.S. Menzies, K.L. Goh, C.C. Jensen, F.B. Gertler, E. Fuchs, R. Fassler, M.C. Beckerle, Targeted disruption of the murine zyxin gene, *Mol. Cell. Biol.* 23 (2003) 70–79.
- [31] W. Witke, A.H. Sharpe, J.H. Hartwig, T. Azuma, T.P. Stossel, D.J. Kwiatkowski, Hemostatic, inflammatory, and fibroblast responses are blunted in mice lacking gelsolin, *Cell* 81 (1995) 41–51.
- [32] W. Hauser, K.P. Knobloch, M. Eigenthaler, S. Gambaryan, V. Krenn, J. Geiger, M. Glazova, E. Rohde, I. Horak, U. Walter, M. Zimmer, Megakaryocyte hyperplasia and enhanced agonist-induced platelet activation in vasodilator-stimulated phosphoprotein knockout mice, *Proc. Natl. Acad. Sci. U. S. A.* 96 (1999) 8120–8125.
- [33] B.E. Drees, K.M. Andrews, M.C. Beckerle, Molecular dissection of zyxin function reveals its involvement in cell motility, *J. Cell Biol.* 147 (1999) 1549–1560.
- [34] U. Gluck, A. Ben Ze'ev, Modulation of alpha-actinin levels affects cell motility and confers tumorigenicity on 3T3 cells, *J. Cell Sci.* 107 (1994) 1773–1782.
- [35] S.N. Nikolopoulos, B.A. Spengler, K. Kisselbach, A.E. Evans, J.L. Biedler, R.A. Ross, The human non-muscle alpha-actinin protein encoded by the ACTN4 gene suppresses tumorigenicity of human neuroblastoma cells, *Oncogene* 19 (2000) 380–386.
- [36] M.G. Nievers, R.B. Birge, H. Greulich, A.J. Verkleij, H. Hanafusa, P.M. van Bergen en Henegouwen, v-Crk-induced cell transformation: changes in focal adhesion composition and signaling, *J. Cell Sci.* 110 (1997) 389–399.
- [37] P. Frontelo, M. Gonzalez-Garrigues, S. Vilaro, C. Gamallo, A. Fabra, M. Quintanilla, Transforming growth factor beta 1 induces squamous carcinoma cell variants with increased metastatic abilities and a disorganized cytoskeleton, *Exp. Cell Res.* 244 (1998) 420–432.
- [38] C.A. Orey, F.M. Pavalko, K. Burridge, An interaction between alpha-actinin and the beta 1 integrin subunit in vitro, *J. Cell Biol.* 111 (1990) 721–729.
- [39] K.A. Knudsen, A.P. Soler, K.R. Johnson, M.J. Wheelock, Interaction of alpha-actinin with the cadherin/catenin cell–cell adhesion complex via alpha-catenin, *J. Cell Biol.* 130 (1995) 67–77.
- [40] W. Birchmeier, J. Behrens, Cadherin expression in carcinomas: role in the formation of cell junctions and the prevention of invasiveness, *Biochim. Biophys. Acta* 1198 (1994) 11–26.
- [41] H.B. Guo, I. Lee, M. Kamar, M. Pierce, N-acetylglucosaminyltransferase V expression levels regulate cadherin-associated homotypic cell–cell adhesion and intracellular signaling pathways, *J. Biol. Chem.* 278 (2003) 52412–52424.
- [42] T.J. Mitchison, L.P. Cramer, Actin-based cell motility and cell locomotion, *Cell* 84 (1996) 371–379.
- [43] R. Zaidel-Bar, C. Ballestrem, Z. Kam, B. Geiger, Early molecular events in the assembly of matrix adhesions at the leading edge of migrating cells, *J. Cell Sci.* 116 (2003) 4605–4613.
- [44] K. Rottner, M. Krause, M. Gimona, J.V. Small, J. Wehland, Zyxin is not colocalized with vasodilator-stimulated phosphoprotein (VASP) at lamellipodial tips and exhibits different dynamics to vinculin, paxillin, and VASP in focal adhesions, *Mol. Biol. Cell* 12 (2001) 3103–3113.
- [45] I. Sadler, A.W. Crawford, J.W. Michelsen, M.C. Beckerle, Zyxin and cCRP: two interactive LIM domain proteins associated with the cytoskeleton, *J. Cell Biol.* 119 (1992) 1573–1587.
- [46] T. Hirota, T. Morisaki, Y. Nishiyama, T. Marumoto, K. Tada, T. Hara, N. Masuko, M. Inagaki, K. Hatakeyama, H. Saya, Zyxin, a regulator of actin filament assembly, targets the mitotic apparatus by interacting with h-warts/LATS1 tumor suppressor, *J. Cell Biol.* 149 (2000) 1073–1086.
- [47] R. Weiskirchen, K. Bister, Suppression in transformed avian fibroblasts of a gene (crp) encoding a cysteine-rich protein containing LIM domains, *Oncogene* 8 (1993) 2317–2324.
- [48] V. Censano, Y. Aalto, S. Perdicchi, G. Bernard, M.C. Manara, S. Benini, G. Cenacchi, P. Preda, G. Lattanzi, B. Nagy, S. Knuutila, M.P. Colombo, A. Bernard, P. Picci, K. Scotlandi, Molecular mechanisms of CD99-induced caspase-independent cell death and cell–cell adhesion in Ewing's sarcoma cells: actin and zyxin as key intracellular mediators, *Oncogene* 23 (2004) 5664–5674.
- [49] D.A. Nix, M.C. Beckerle, Nuclear-cytoplasmic shuttling of the focal contact protein, zyxin: a potential mechanism for communication between sites of cell adhesion and the nucleus, *J. Cell Biol.* 138 (1997) 1139–1147.
- [50] Y.Y. Degenhardt, S. Silverstein, Interaction of zyxin, a focal adhesion protein, with the e6 protein from human papillomavirus type 6 results in its nuclear translocation, *J. Virol.* 75 (2001) 11791–11802.
- [51] H. Hasle, M. Arico, G. Basso, A. Biondi, R.A. Cantu, U. Creutzig, S. Fenu, C. Fonatsch, O.A. Haas, J. Harbott, G. Kardos, G. Kemdrup, G. Mann, C.M. Niemeyer, H. Ptoszkova, J. Ritter, R. Slater, J. Stary, B. Stollmann-Gibbels, A.M. Testi, E.R. van Wering, M. Zimmermann, Myelodysplastic syndrome, juvenile myelomonocytic leukemia, and acute myeloid leukemia associated with complete or partial monosomy 7, European Working Group on MDS in Childhood (EWOG-MDS), *Leukemia* 13 (1999) 376–385.
- [52] B. Johansson, F. Mertens, F. Mitelman, Cytogenetic deletion maps of hematologic neoplasms: circumstantial evidence for tumor suppressor loci, *Genes Chromosomes Cancer* 8 (1993) 205–218.
- [53] S. Tosi, J. Harbott, O.A. Haas, A. Douglas, D.M. Hughes, F.M. Ross, A. Biondi, S.W. Scherer, L. Kearney, Classification of deletions and identification of cryptic translocations involving 7q by fluorescence in situ hybridization (FISH), *Leukemia* 10 (1996) 644–649.
- [54] M.M. LeBeau, R. Espinosa III, E.M. Davis, J.D. Eisenbart, R.A. Larson, E.D. Green, Cytogenetic and molecular delineation of a region of chromosome 7 commonly deleted in malignant myeloid diseases, *Blood* 88 (1996) 1930–1935.